Challenge Journal of
STRUCTURAL MECHANICS

Vol.9 No.2 (2023)

auxetic building codes compressive strength dynamic analysis earthquake finite element analysis finite element method girder bridge mechanical properties metaheuristic algorithms modal analysis optimization prestresing pushover analysis reinforced concrete seismic design shallow foundations smart concrete steel structures structural dynamics temperature effects thick plate wind

TULPAR ACADEMIC PUBLISHING

ISSN 2149-8024

Challenge Journal of Structural Mechanics

EDITOR-IN-CHIEF

Assoc. Prof. Dr. Fatih Mehmet ÖZKAL
Atatürk University, Türkiye

CO-EDITOR-IN-CHIEF

Assoc. Prof. Dr. Serdar ÇARBAŞ
Karamanoğlu Mehmetbey University, Türkiye

EDITORIAL BOARD

Prof. Dr. A. Ghani RAZAQPUR
McMaster University, Canada

Prof. Dr. Paulo B. LOURENÇO
University of Minho, Portugal

Prof. Dr. Gilbert Rainer GILLICH
Eftimie Murgu University of Resita, Romania

Prof. Dr. Long-Yuan LI
University of Plymouth, United Kingdom

Prof. Dr. Željana NIKOLIĆ
University of Split, Croatia

Prof. Dr. Habib UYSAL
Atatürk University, Türkiye

Prof. Dr. Filiz PİROĞLU
İstanbul Technical University, Türkiye

Prof. Dr. Alper BÜYÜKKARAGÖZ
Gazi University, Türkiye

Assoc. Prof. Dr. Bing QU
California Polytechnic State University, United States

Assoc. Prof. Dr. Naida ADEMOVIĆ
University of Sarajevo, Bosnia and Herzegovina

Assoc. Prof. Dr. Anna SAETTA
IUAV University of Venice, Italy

Prof. Dr. Halil SEZEN
The Ohio State University, United States

Prof. Dr. Adem DOĞANGÜN
Uludağ University, Türkiye

Prof. Dr. M. Asghar BHATTI
University of Iowa, United States

Prof. Dr. Reza KIANOUSH
Ryerson University, Canada

Prof. Dr. Y. Cengiz TOKLU
Beykent University, Türkiye

Prof. Dr. Togay ÖZBAKKALOĞLU
Texas State University, United States

Prof. Dr. Mehmet ÖZYAZICIOĞLU
Atatürk University, Türkiye

Assoc. Prof. Dr. Khaled MARAR
Eastern Mediterranean University, Cyprus

Assoc. Prof. Dr. Hong SHEN
Shanghai Jiao Tong University, China

Assoc. Prof. Dr. Nunziante VALOROSO
Parthenope University of Naples, Italy

Assoc. Prof. Dr. Taha IBRAHIM
Benha University, Egypt

Assoc. Prof. Dr. Amin GHANNADIASL
University of Mohaghegh Ardabili, Iran

Dr. Sandro CARBONARI
Marche Polytechnic University, Italy

Dr. Chien-Kuo CHIU
National Taiwan University of Science and Technology, Taiwan

Dr. Teng WU
University at Buffalo, United States

Dr. Pierfrancesco CACCIOLA
University of Brighton, United Kingdom

Dr. Marco CORRADI
University of Perugia, Italy

Dr. José SANTOS
University of Madeira, Portugal

Dr. Luca LANDI
University of Bologna, Italy

Dr. Mirko MAZZA
University of Calabria, Italy

Dr. Süleyman Nazif ORHAN
Erzurum Technical University, Türkiye

Dr. Casim YAZICI
Ağrı İbrahim Çeçen University, Türkiye

Assoc. Prof. Dr. Oğuz Akın DÜZGÜN
Atatürk University, Türkiye

Dr. Zühal ÖZDEMİR
The University of Sheffield, United Kingdom

Dr. Syahril TAUFIK
Lambung Mangkurat University, Indonesia

Dr. J. Michael GRAYSON
The Citadel - The Military College of South Carolina, United States

Dr. Fabio MAZZA
University of Calabria, Italy

Dr. Alberto Maria AVOSSA
Second University of Naples, Italy

Dr. Susanta GHOSH
Michigan Technological University, United States

Dr. Burak Kaan ÇIRPICI
Erzurum Technical University, Türkiye

Dr. Panatchai CHETCHOTISAK
Rajamangala University of Technology Isan, Thailand

Dr. Chitaranjan PANY
Vikram Sarabhai Space Centre, India

Dr. Ehsan HARIRCHIAN
Bauhaus-Universität Weimar, Germany

E-mail: *cjsmec@challengejournal.com*

Web page: *cjsmec.challengejournal.com*

TULPAR Academic Publishing
www.tulparpublishing.com

Challenge Journal of Structural Mechanics

CONTENTS

Research Articles

TULPAR ACADEMIC PUBLISHING

Challenge Journal of Structural Mechanics

Research Article

Methods for multi-segment continuous cable analysis

Abdullah Demir [a,*], Uğur Polat [b]

[a] *Department of Civil Engineering, Abdullah Gül University, 38080 Kayseri, Türkiye*
[b] *Department of Civil Engineering, Middle East Technical University, 06800 Ankara, Türkiye*

ABSTRACT

Cables are invaluable members for some applications of engineering. The specialty is due to its behavior under transverse loads. Having almost no rigidity in transverse direction makes cables different from other structural elements. In most applications, cables are assumed to be two force members. However, not only its weight but also its application with roller supports makes them different structural elements. Generally, cables are assembled as single-segmented cables (SSC) where they are fixed at their ends. However, in most of the SSC applications, cables have intermediate supports which can be rollers or sliders. These type of cable applications are called as multi-segment continuous cables (MSCC). In MSCC systems, the cable fixed at its ends and supported by a number of intermediate rollers. Total length of cable is constant, and the intermediate supports are assumed to be frictionless and stationary. In this problem, the critical issue is to find the distribution of the cable length among the segments in the final equilibrium state, so reactions at all supports can be found. Two methods are proposed for the segment length adjustment based on the stress continuity among the cable. These methods are named as direct stiffness method and tension distribution method (relaxation method). Results calculated from the proposed methods are verified by both the reference benchmark problems and commercial finite element program.

ARTICLE INFO

Article history:
Received 22 August 2022
Revised 27 October 2022
Accepted 11 January 2023

Keywords:
Tensegrity
Single-segment cable
Multi-segment cable
Direct stiffness method
Tension distribution method

1. Introduction

Cables are invaluable elements for structural systems such as guyed towers, cable-stayed bridges marine vehicles, offshore structures, cable roofs, tensegrities, transmission lines and pre-stressing works. Cables can be bended without any residual stress. This property makes them more nonlinear than other structural elements. Although, the nonlinearity is both geometric and material, material nonlinearity is not considered (Judge et al. 2012; Prawoto and Mazlan 2012) in the scope of this research.

Various single-segment cable (SSC) analysis methods have been proposed by researchers. These methods solve the continuous cable fixed at both ends. Some researchers (Dischinger 1949; Ernst 1965) made some shape predictions for cable which is generalized in the research of Hajdin et al. (1998) and some made finite element calculations with iterative procedures which is pioneered by Micholas and Brinstiel (1962) and Skop and O'Hara (1970). After increase of computational capabilities in 1980's, researchers have proposed methods for more accurate results. Peyrot and Goulois (1979) proposed a finite element solution procedure for cable considering its catenary action. Polat (1981) applied Newton-Raphson method to the nonlinearity of cable problems. Fleming (1979) and Ren et al. (2008) proposed different finite element procedures to solve cable structures. Force density method was also used by Christou et al. (2014) for implementation of slack cables. Besides, author used (Dinçer and Demir 2020) Smoothed particle hydrodynamics (SPH), which is a meshless method, for analysis of single segment cable.

Although there are many studies about SSC analysis, limited researches have made for multi-segment continuous cables (MSCC). Some solution methods for cable systems having more than one segment were proposed

* *Corresponding author*. Tel.: +90-312-210-2401 ; Fax: +90-312-210-5401 ; E-mail address: abdullah.demir@agu.edu.tr (A. Demir)
ISSN: 2149-8024 / DOI: https://doi.org/10.20528/cjsmec.2023.02.001

in the following studies. Aufaure (1993, 2000) defined a cable system having two segments. In that study, a cable was fixed at both ends and supported by one roller support. The cable was analyzed with a finite element method in which a specific element was defined. This finite element was the contact element of cable with roller support. Three nodes named as N1, N2, N3 were defined on this element in which N3 is the intermediate one. Position of N3 must be in between N1 and N2 and it is found by stress continuity through the cable. A similar method with sliding cable elements was proposed by Zhou et al. (2004). Ju and Choo (2005) are proposed a super element approach. Although frictional effect between cables and pulleys was taken into consideration, cable was assumed to be a linear structural element in that study. McDonald and Peyrot (1988, 1990) studied on cables suspended in sheaves. They used a cable element based on a catenary relationship and defined a pulley element in their study. Besides, a dynamic relaxation formulation was given for tensegrity structures by Bel Hadj Ali et al. (2017). Element free Galerkin method was also used for solution of membranes strengthen by sliding cable in research of Noguchi (2004) and Dehghan and Abbaszadeh (2016).

In this study, a novel method is proposed for the solution of multi-segment continuous cable analysis. Solution of continuous cable is achieved by dividing the complete cable system into segments. Each single-segment cable is solved by the method proposed by Polat (1981). This method is redefined for the sake of completeness of the research. Then, the direct stiffness and tension distribution method is defined (Demir 2011). Methods are verified by benchmark problems and commercial finite element solver (ANSYS).

2. Methodology

2.1. Single segment cable (SSC) analysis

Cable fixed at one end is a determinant system and the second end of cable has a position for the corresponding reaction at the first end. Reaction at the first end is changed by some iteration techniques until the released end of cable is positioned at desired location, which is the second fixed support. A detailed formulation of SSC analysis for 2D and 3D can be seen in the studies of Polat (1981) and Demir (2011), respectively.

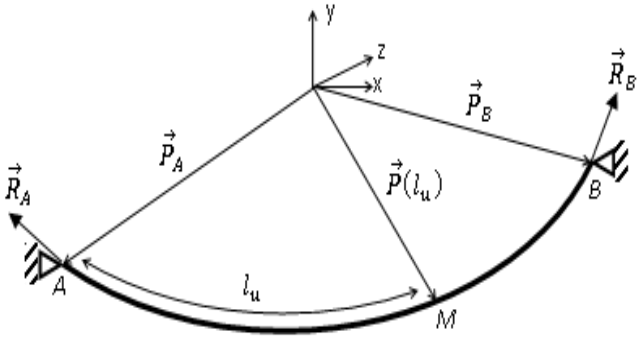

Fig. 1. An SSC layout.

In an SSC as illustrated in Fig. 1, position of an arbitrary node M can be defined as;

$$\vec{P}(l_u) = \vec{P}_A - \int_0^{l_u} \frac{\vec{R}(s)}{T(s)}[1+\varepsilon(s)]ds \tag{1}$$

where $\vec{P}_A$ is the position vector of A, l_u is the cable length from A to M, $\vec{R}(s)$ $T(s)$ and $\varepsilon(s)$ are the reaction vector, tension and strain at s, respectively.

The relation between change in position of node B, $\Delta\vec{P}_B$, and change in reaction at node A, $\Delta\vec{R}_A$, can be expressed with the help of tangent stiffness matrix $[S]$.

$$\Delta\vec{R}_A = [S]\Delta\vec{P}_B \tag{2}$$

From Equation (1) $\Delta\vec{P}_B$ is determined as;

$$\Delta\vec{P}_B = -\int_0^{L_u}\left\{\left|\frac{1+\varepsilon(l_u)}{T(l_u)}\right|\Delta\vec{R}_A - \left|\frac{1+(1-\upsilon)\varepsilon(l_u)}{T^3(l_u)}\right|[\vec{R}(l_u)\cdot\Delta\vec{R}_A]\vec{R}(l_u)\right\}dl_u \tag{3}$$

where υ is Poissson's ratio.

In global coordinate directions, Eq. (3) can be expressed in Cartesian coordinate directions as;

$$\Delta P_{BX}\hat{\imath} = -\int_0^{L_u}[C_1\Delta R_{AX}\hat{\imath} - C_2C_3C_4]\,dl_u \tag{4a}$$

$$\Delta P_{BY}\hat{\jmath} = -\int_0^{L_u}[C_1\Delta R_{AY}\hat{\jmath} - C_2C_3C_4]\,dl_u \tag{4b}$$

$$\Delta P_{BZ}\hat{k} = -\int_0^{L_u}\left[C_1\Delta R_{AZ}\hat{k} - C_2C_3C_4\right]dl_u \tag{4c}$$

where

$C_1 = \left[\frac{1+\varepsilon(l_u)}{T(l_u)}\right]$,

$C_2 = \left[\frac{1+(1-\upsilon)\varepsilon(l_u)}{T^3(l_u)}\right]$,

$C_3 = [R_X(l_u)\Delta R_{AX} + R_Y(l_u)\Delta R_{AY} + R_Z(l_u)\Delta R_{AZ}]$, and

$C_4 = \left[R_X(l_u)\hat{\imath} + R_Y(l_u)\hat{\jmath} + R_Z(l_u)\hat{k}\right]$.

where ΔP_{BX}, ΔP_{BY} and ΔP_{BZ} are directional components of $\Delta\vec{P}_B$ as for $\Delta\vec{R}_A$, L_u is total unstressed length of cable, $R_X(l_u)$, $R_Y(l_u)$ and $R_Z(l_u)$ are directional components of $\vec{R}(l_u)$.

Writing Eqs. (4a), (4b) and (4c) in the form of Eq. (2);

$$\begin{Bmatrix}\Delta P_{BX}\\ \Delta P_{BY}\\ \Delta P_{BZ}\end{Bmatrix} = [S]^{-1}\begin{Bmatrix}\Delta R_{AX}\\ \Delta R_{AY}\\ \Delta R_{AZ}\end{Bmatrix} \tag{5}$$

where

$$[S] = \begin{bmatrix} -\int_0^{L_u}[C_1 - C_2R_X^2(l_u)]\,dl_u & -\int_0^{L_u}[C_2R_X(l_u)R_Y(l_u)]\,dl_u & -\int_0^{L_u}[C_2R_X(l_u)R_Z(l_u)]\,dl_u \\ -\int_0^{L_u}[C_2R_Y(l_u)R_X(l_u)]\,dl_u & -\int_0^{L_u}[C_1 - C_2R_Y^2(l_u)]\,dl_u & -\int_0^{L_u}[C_2R_Y(l_u)R_Z(l_u)]\,dl_u \\ -\int_0^{L_u}[C_2R_Z(l_u)R_X(l_u)]\,dl_u & -\int_0^{L_u}[C_2R_Z(l_u)R_Y(l_u)]\,dl_u & -\int_0^{L_u}[C_1 - C_2R_Z^2(l_u)]\,dl_u \end{bmatrix} \tag{6}$$

An iterative solution of Eq. (5) gives the solution for SSC. Results of SSC are important because MSCC analysis is based on it, which means that obtaining correct SSC results will calibrate the MSCC analysis. This relation is more apparent in MSCC part. Two reference case (in part 3) are used to validate the results of SSC.

2.2. Direct stiffness method (DSM)

Multi-segment continuous cables are monolithic structural elements like continuous beams. In MSCC system there are number of intermediate supports. These supports are stationary and frictionless. Thus, cable is free to slide over these intermediate supports. In addition to the assumption of zero friction, intermediate rollers are assumed to be points. Thus, cable finds its stationary position by sliding on the roller supports i.e. changing length of cable at each segment. Direct stiffness method is developed by modeling this inherent sliding motion.

Total cable length of a MSCC system is known. However, length of each segment is unknown. Therefore, solution procedure of MSCC system starts with distribution of total cable length to each segment. In Fig. 2, an initial geometry of MSCC is given with defined unstressed segment lengths l_u^i, where i is the segment number.

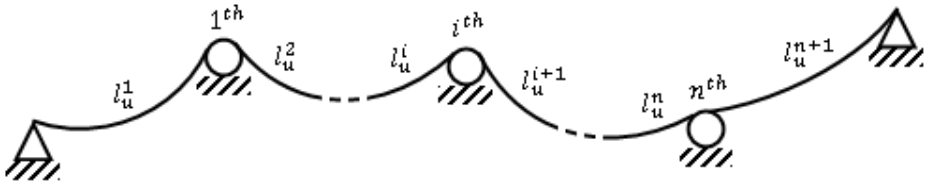

Fig. 2. Configuration of an MSCC system.

Summation of each unstressed cable length gives the total length of the continuous cable with n segments.

$$L_u = \sum_{i=1}^{n} l_u^i \tag{7}$$

Solution of each cable segment is performed by SSC procedure with its known cable length. SSC solution for each segment gives the forces at the ends of the segments. Wrong distribution of segmental lengths will lead to unbalanced forces on intermediate roller supports. The unbalanced forces at i^{th} roller support (i^{th} roller support is the connection point of i^{th} segment and $(i+1)^{th}$ segment) is shown in Eq. (8) as ΔT^i.

$$\Delta T^i = \left|\vec{R}_F^{i+1}\right| - \left|\vec{R}_L^i\right| \tag{8}$$

where $\vec{R}_F^{i+1}$ and $\vec{R}_L^i$ are shown in **Hata! Başvuru kaynağı bulunamadı.**.

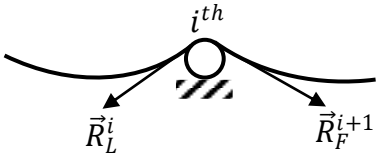

Fig. 3. FBD of a roller support of an MSCC system.

Converging to balanced support reactions is possible only by correct prediction. If not, correction step is needed for segment lengths of cable. Assuming quasilinear behavior of the system at the end of each predictive solution step, a relation between unstressed length adjustment Δl_u^j and corresponding change in the unbalanced reactions ΔT^i can be set up; where i and j denotes the support number. The relation is expressed in matrix form as follows.

$$\{\Delta T\} = [K] \cdot \{\Delta l_u\} \tag{9}$$

where, ΔT is a $(nx1)$ vector composed of ΔT^i, Δl_u is a (n x 1) vector composed of Δl_u^j, K is a (n x n) coefficient matrix composed of K_{ij}.

Coefficient matrix can be regarded as a tangential stiffness matrix in which K_{ij} represents the change in unbalanced reaction, δT^i, due to a change in unstressed length δl_u^j between cable segments j and $(j+1)$. The tangential stiffness matrix in Eq. (9) can be constructed column-by-column by adjusting the unstressed lengths of cable segments at support j by a small amount δl^j and calculating the resulting changes in the unbalanced reactions δT^i at all supports from the reanalysis of the SCC with the changed segment lengths. The j^{th} column of $[K]$ is obtained as.

$$\begin{Bmatrix} K_1 \\ \vdots \\ K_i \\ \vdots \\ K_n \end{Bmatrix} = \begin{Bmatrix} \delta T^1/\delta l^j \\ \vdots \\ \delta T^i/\delta l^j \\ \vdots \\ \delta T^n/\delta l^j \end{Bmatrix} \tag{10}$$

The objective is to balance the reactions at supports which is the static equilibrium condition. This is possible by applying required length adjustment for each segment. Length adjustments are achieved by solving Eq. (9). If the cable behavior were linear, the length adjustments $\{\delta l_u\}$ would eliminate the unbalanced reactions at intermediate supports and bring the cable system into true equilibrium. However, iterations are needed for the final equilibrium due to nonlinear behavior of cable. Newton-Raphson method is implemented for this predictive/corrective algorithm to reach the final equilibrium state.

2.3. Tension distribution method (TDM) (relaxation method)

Tension distribution method is a special form of the direct stiffness method. Being inception of analysis, TDM is inspired from the moment distribution method which is commonly used for the analysis of continuous beams. Relaxation method is the byname of this method. This additional name is given due to relaxation procedure at supports while balancing the reactions of cables at supports. In this context, this method is similar to DSM. The

basic difference is the way of relaxation. While segment lengths are incremented for the whole system in DSM, slip amount is determined for two adjacent segments in TDM. Therefore, in the corrective stage, an influence (stiffness) coefficient is calculated at a selected joint first by introducing a virtual adjustment at the joint. Thus, the actual amount of adjustment required to eliminate the unbalanced reaction at the joint is determined based on this information. A cyclic procedure is needed for TDM, because elimination of unbalanced reactions (relaxation) is made for one support. Therefore, iterative cyclic calculations are carried out until the unbalanced reactions at the intermediate supports became negligibly small.

It is expected that; application of anticipated length adjustment Δl_u^i, for i^{th} roller support makes the tension difference ΔT^i, zero. Relation between Δl_u^i and ΔT^i is expressed in Eq. (11).

$$\Delta T^i = k^i \Delta l_u^i \tag{11}$$

The stiffness coefficient of the i^{th} roller support k^i, can be found by adjusting the unstressed lengths of adjacent segments by applying a small amount δl_u^i and calculating the resulting changes in the unbalanced reactions δT^i at that support as follows.

$$k^i = \delta T^i \Big/ \delta l_u^i \tag{12}$$

In correction step of calculations, length adjustments can be calculated by the known tension difference ΔT^i and stiffness coefficient k^i from Eq. (11). It is not expected that; unbalanced reactions on each roller support to be zero in a single cycle of correction step due to nonlinear behavior of cable. Therefore, Newton-Raphson iterations are used to handle that nonlinearity.

In order to verify and prove the result of both methods, a benchmark cable system is created for MSCC system to point out the effect of cable motion on rollers.

3. Verification Cases

3.1. Case 1

Case 1 is a benchmark problem which is used by many researchers (Andreu et al. 2006; Jayaraman and Knudson 1962; Michalos and Birnstiel 1962; O'Brien and Francis 1964; Salehi et al. 2013; Thai and Kim 2011; Tibert 1999; Yang and Tsay 2007). A cable suspended by two fixed supports has its catenary shape as illustrated in Fig. 4. Initial properties of cable are given in Table 1. An external concentrated load is applied, and displacements of this node is determined. Results are comparatively shown in Table 2.

3.2. Case 2

Another SSC was defined by Peyrot and Goulois (1979) and used by researchers (Salehi et al. 2013; Yang and Tsay 2007). In this case, one end of the cable is fixed at a fixed position (0 m, 90 m) and the other end is moved starting from (0 m, 30 m) to (100 m, 30 m) as seen in Fig. 5. Initial properties of problem are given in Table 3. Reactions at the second end of the cable is compared as seen in Table 4.

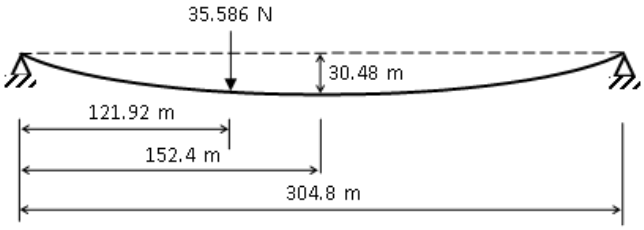

Fig. 4. SSC under concentrated load.

Table 1. Initial properties of Case 1.

Item	Data
Cable self-weight	46.12 N/m
Cross-sectional area	548.4 mm²
Elastic modulus	131 kN/mm²
Sag under self-weight at load point	29.262 m
Unstressed cable length 1-2	125.88 m
Unstressed cable length 2-3	186.85 m

Table 2. Comparison of results of Case 1.

Researcher	Vertical displacement (m)	Horizontal displacement (m)
Michalos and Birnstiel (1962)	-5.472	-0.845
Jayaraman and Knudson (1962)	-5.626	-0.859
Yang and Tsay (2007)	-5.625	-0.859
Thai and Kim (2011)	-5.626	-0.859
Andreu et al. (2006)	-5.626	-0.860
O'Brien and Francis (1964)	-5.627	-0.860
Tibert (1999)	-5.626	-0.859
Salehi et al. (2013)	-5.592	-0.855
SSC Solution	-5.626	-0.859

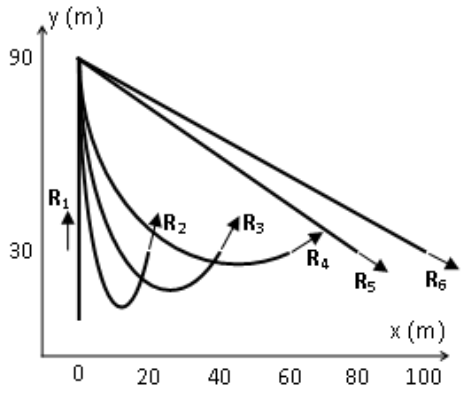

Fig. 5. SSC configuration of Case 2.

Table 3. Initial properties of Case 2.

Item	Data
Unstressed cable length	100 m
Cross-sectional area	1 m²
Cable self-weight	1 N/m
Elastic modulus	3.0e7 N/mm²
Thermal expansion coefficient	0.65e-5 1/°K
Thermal change	100°K

3.3. Case 3

In order to configure a multi segment continuous cable, a continuous cable is fixed at its ends ((0,0) and (300,0)) and supported by two rollers ((100,0) and (200,0)). All supports are positioned at the same elevation to point out the load effect on change in segmental lengths. Total cable length is selected longer than the total direct distance between supports, hereby a slack cable is achieved. Initially, the cable is loaded under its self-weight and a distributed load which is the ten times unit cable weight. This distributed load is applied on mid one fifth portion of whole cable. Initial properties of system are given in Table 5 and initial equilibrium state under self-weight and external distributed load is given in Fig. 6.

In this state, cable is almost linear at the first and the third segment. Theoretically, cable lengths at these segments should be equal due to symmetry. Taking maximum error as 0.1 mm and 0.1 N, cable lengths for each segment are given for finite element numbers in Fig. 7. As seen, almost same cable lengths are achieved for a small number of elements. In addition, maximum displacements at the midpoint of mid-segment are given for increasing number of elements in Fig. 8.

Table 4. The reactions at the second end of the cable.

Researchers	Peyrot and Goulois (1979)		Yang and Tsay (2007)		Salehi et al. (2013)		SSC Solution	
Reactions	x	y	x	y	x	y	x	y
R1	0.00	20.02	0.01	20.02	0.01	19.99	0.0	20.02
R2	3.061	19.93	3.061	19.93	3.090	19.83	3.061	19.942
R3	9.172	19.24	9.172	19.24	9.16	19.14	9.172	19.252
R4	22.15	15.73	22.15	15.73	22.11	15.63	22.146	15.744
R5	504.0	-328	504.1	-328.9	504.48	-329.4	504.102	-328.859
R6	4.17e6	2.511e6	42.56e6	-25.53e6	42.56e6	-25.55e6	42.58e6	-25.55e6

Table 5. Initial properties of Case 3.

Item	Data
Total unstressed cable length	315 m
Cross-sectional area	7.854e-5 m²
Cable self-weight	6.0482 N/m
External load	60.482 N/m
Elastic modulus	200e9 N/m²
Thermal expansion coefficient	1.2e-5 1/C

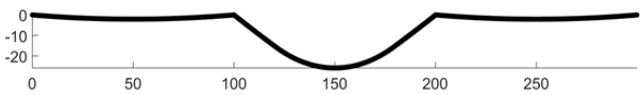

Fig. 6. Initial equilibrium state of Case 3.

In this state, cable is almost linear at the first and the third segment. Theoretically, cable lengths at these segments should be equal due to symmetry. Taking maximum error as 0.1 mm and 0.1 N, cable lengths for each segment are given for finite element numbers in Fig. 7. As seen, almost same cable lengths are achieved for a small number of elements. In addition, maximum displacements at the midpoint of mid-segment are given for increasing number of elements in Fig. 8.

Additional point loads are applied to see the changes in cable lengths of segments and the displacement of mid-segment. These point loads are applied to left segment and right segment. Amounts of point loads are 5080.488 N and 2540.488 N, respectively. Locations of forces on cable are specified as cable length which are 63 m and 252 m measured from left support of MSCC system. Final configuration of MSCC is given in Fig. 9 for 3000 finite elements and predefined precisions. Changes on MSCC system solved by TDM, DSM and ANSYS (a commercial computer program) are given in Tables 6-8, respectively. Solution times does not exceed a several minutes via a standard laptop computer. Solution time depends on mostly the cable slackness which decreases its stability. In ANSYS analysis, LINK10 element is used to model the cable. Besides, CONTA175 and TARGE169 elements are used for modelling of contact between the roller and the cable.

Table 6. Coordinates of nodes having maximum vertical displacement solved by TDM.

Segments	Initial state		Final state	
	X (m)	Y (m)	X (m)	Y (m)
Left segment	50	-2.0640	59.0275	-22.2794
Mid-segment	149.8866	-25.8670	148.6932	-11.5097
Right segment	250	-2.0798	237.8608	-10.4961

Table 7. Coordinates of nodes having maximum vertical displacement solved by DSM.

Segments	Initial state		Final state	
	X (m)	Y (m)	X (m)	Y (m)
Left segment	50	-2.0723	59.0277	-22.2806
Mid-segment	149.8866	-25.8670	148.6931	-11.5098
Right segment	250	-2.0798	237.8608	-10.4961

Table 8. Coordinates of nodes having maximum vertical displacement solved by ANSYS.

Segments	Initial state		Final state	
	X (m)	Y (m)	X (m)	Y (m)
Left segment	50	-2.0712	58.9193	-22.2874
Mid-segment	149.9024	-25.9248	148.6820	-11.5099
Right segment	250	-2.0768	237.7980	-10.4932

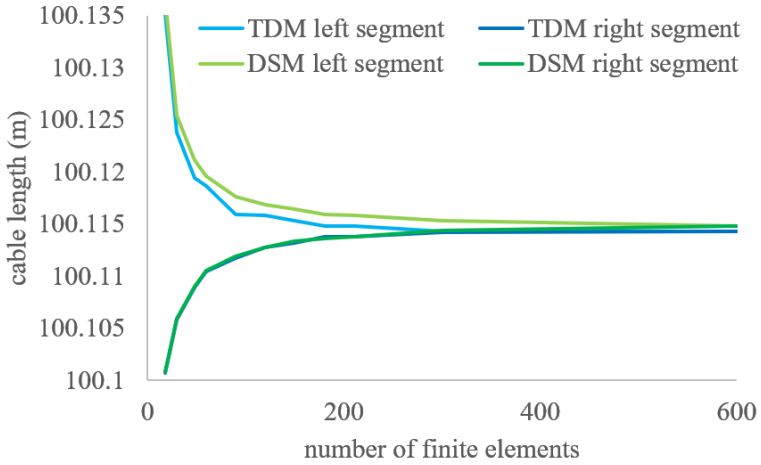

Fig. 7. Segment cable lengths vs. number of finite elements.

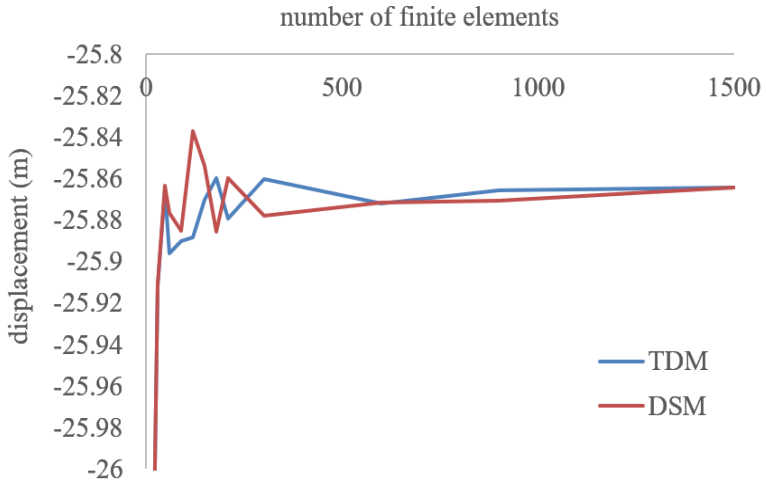

Fig. 8. Maximum displacement vs. number of finite elements.

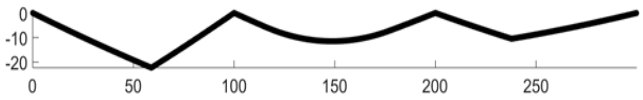

Fig. 9. Final equilibrium state of Case 3.

4. Conclusions

Multi-segment continuous cable (MSCC) has different behavior from single segment cable (SSC). A cable having constant length is fixed at its ends in SSC systems. In contrast, a cable having constant length is fixed at ends and supported by stationary and frictionless roller supports between ends in MSCC systems. Therefore, cable length of each segment is not constant for MSCC; it can change by the change of loading conditions as seen in the verification cases. This length change will change the resultant forces on cable and supports.

In this study, a novel solution approach is proposed for MSCC systems. Two methods are proposed; direct stiffness method (DSM) and tension distribution method (TDM) (relaxation method). DSM is imitated from the inherent motion of cable on roller supports and based on the stress continuity on the continuous cable. TDM is inspired from the moment distribution method, which has been used for continuous beam solutions.

DSM calculates length adjustment for the entire system consisting all segments which yields stress continuity through the cable. Length adjustments are calculated and applied for all roller supports. Nevertheless, stress continuity does not yield in one calculation phase. TDM calculates the length adjustment for two adjacent segments. Length adjustments are calculated and applied for each roller support, thus one cycle of calculations is fulfilled. Nevertheless, stress continuity does not yield in one cycle due to nonlinear behavior of cable. Newton-Raphson technique is used for both methods to overcome the nonlinearity.

Although DSM and TDM run in a similar manner, there are some differences. Those differences are due to the behavior of methods. DSM considers the circumstances on each segment while calculating the segment length adjustments. In contrast, TDM adjust two adjacent segment lengths by assuming other segments ineffective. Thus, those behaviors of methods give some advantages and disadvantages which are mainly related with the computational cost of the methods. DSM loses its effectiveness and speed for cable systems having many segments. In contrast, speed (not solution time) of TDM does not depend on the number of roller supports. Consequently, selection of method should be made accordingly, which will affect the solution time. Nevertheless, verification results show that both methods are effective and accurate methods for MSCC systems.

Acknowledgements

None declared.

Funding

The authors received no financial support for the research, authorship, and/or publication of this manuscript.

Conflict of Interest

The authors declared no potential conflicts of interest with respect to the research, authorship, and/or publication of this manuscript.

References

Andreu A, Gil L, Roca P (2006). A new deformable catenary element for the analysis of cable net structures. *Computer & Structures*, 84(29–30), 1882–1890.

Aufaure M (1993). A finite element of cable passing through a pulley. *Computers & Structures*, 46(5), 807–812.

Aufaure M (2000). Three-node cable element ensuring the continuity of the horizontal tension; A clamp-cable element. *Computers and Structures*, 74(2), 243–251.

Bel Hadj Ali N, Sychterz AC, Smith IF C (2017). A dynamic-relaxation formulation for analysis of cable structures with sliding-induced friction. *International Journal of Solids and Structures*, 126–127, 240–251.

Christou P, Michael A, Elliotis M (2014). Implementing slack cables in the force density method. *Engineering Computations (Swansea, Wales)*, 31(5), 1011–1030.

Dehghan M, Abbaszadeh M (2016). Analysis of the element free Galerkin (EFG) method for solving fractional cable equation with Dirichlet boundary condition. *Applied Numerical Mathematics*, 109, 208–234.

Demir A (2011). Form Finding and Structural Analysis of Cables with Multiple Supports. *M.Sc. thesis*. Middle East Technical University, Ankara.

Dinçer AE, Demir A (2020). Application of smoothed particle hydrodynamics to structural cable analysis. *Applied Sciences*, 10(24), 8983.

Dischinger F (1949). Hängebrücken fur schwerste verkehrslasten. *Der Bauingenieur*, 24, 65–107.

Ernst HJ (1965). Der E-modul von seilen unter brucksichtigung des durchhangers. *Der Bauingenieur*, 40(2), 52–55.

Fleming JF (1979). Nonlinear static analysis of cable-stayed bridge structures. *Computers & Structures*, 10(4), 621–635.

Hajdin N, Michaltsos GT, Konstantakopoulos TG (1998). About the equivalent modulus of elasticity of cables of cable-stayed bridges. *Facta Universitatis Series : Architecture and Civil Engineering*, 1(5), 569–575.

Jayaraman HB, Knudson WC (1962). A curved element for the analysis of cabe structures. *Transactions of the American Society of Civil Engineers*, 127, 267–281.

Ju F, Choo YS (2005). Super element approach to cable passing through multiple pulleys. *International Journal of Solids and Structures*, 42(11–12), 3533–3547.

Judge R, Yang Z, Jones SW, Beattie G (2012). Full 3D finite element modelling of spiral strand cables. *Construction and Building Materials*, 35, 452–459.

McDonald BM, Peyrot AH (1988). Analysis of cables suspended in sheaves. *Journal of Structural Engineering*, 114(3), 693–706.

McDonald BM, Peyrot AH (1990). Sag-tension calculations valid for any line geometry. *Journal of Structural Engineering*, 116(9), 2374–2386.

Michalos J, Birnstiel C (1962). Movements of a cable due to changes in loading. *Transactions of the American Society of Civil Engineers*, 127, 267–281.

Noguchi H, Kawashima T (2004). Meshfree analyses of cable-reinforced membrane structures by ALE–EFG method. *Engineering Analysis with Boundary Elements*, 28(5), 443–451.

O'Brien WT, Francis AJ (1964). Cable movements under two-dimensional loads. *Journal of Structural Division ASME*, 90, 89–124.

Peyrot AH, Goulois AM (1979). Analysis of cable structures. *Computers and Structures*, 10(5), 805–813.

Polat U (1981). Nonlinear Computer Analysis of Guyed Towers and Cables. *M.Sc. thesis.* Middle East Technical University, Ankara.

Prawoto Y, Mazlan RB (2012). Wire ropes: Computational, mechanical, and metallurgical properties under tension loading. *Computational Materials Science*, 56, 174–178.

Ren W-X, Huang M-G, Hu W-H (2008). A parabolic cable element for static analysis of cable structures. *Engineering Computations: Int J for Computer-Aided Engineering*, 25, 366–384.

Salehi AAM, Shooshtari A, Esmaeili V, Naghavi Riabi A (2013). Nonlinear analysis of cable structures under general loadings. *Finite Elements in Analysis and Design*, 73, 11–19.

Skop RA, O'Hara GJ (1970). The method of imaginary reactions: a new technique for analyzing structural cable systems. *Marine Technology Society Journal*, 4(1), 21–30.

Thai H-TT, Kim S-EE (2011). Nonlinear static and dynamic analysis of cable structures. *Finite Elements in Analysis and Design*, 47(3), 237–246.

Tibert G (1999). *Numerical analyses of cable roof structures*. KTH.

Yang YB, Tsay J-Y (2007). Geometric nonlinear analysis of cable structures with a two-node cable element by generalized displacement control method. *International Journal of Structural Stability and Dynamics*, 7(4), 571–588.

Zhou B, Accorsi ML, Leonard JW (2004). Finite element formulation for modeling sliding cable elements. *Computers and Structures*, 82(2–3), 271–280.

Challenge Journal of Structural Mechanics

Research Article

Turkey's disaster and emergency profile: Settlement information and analysis of earthquake parameters

Fahri Birinci [a,*]

[a] *Department of Civil Engineering, Ondokuz Mayıs University, 55139 Samsun, Türkiye*

ABSTRACT

Thousands of people die and billions of dollars of financial loss occur every year in Turkey and the world due to natural disasters. Although many reports and regulations have been prepared to eliminate the negative situations caused by natural disasters, changing climate conditions, technological advances and social habits require these measures to be developed, renewed, and made sustainable over time. In this context, creating a data pool to prevent the loss of life and property caused by disasters and performing the necessary studies becomes even more important. In addition to disaster-related information, this data pool should include physical and geographic information such as the distances of people's communal living areas to the administrative centers, the population in these living areas, and transportation facilities. In this study, a disaster and emergency profile for Turkey has been tried to be presented. For this, the distances of all settlements to the districts and provincial centers they are connected to, the transportation times and speeds of these centers, the altitudes of the settlements, earthquake zone numbers, earthquake hazard map parameters, populations, and areas were compiled or calculated. The evaluation was made separately according to the districts and provinces, taking into account the determined limits. Based on the profile reached at the end of the study, suggestions were developed for planning and projects for disasters and emergencies.

ARTICLE INFO

Article history:
Received 7 November 2022
Revised 17 January 2023
Accepted 3 March 2023

Keywords:
Disasters and emergencies
Earthquake hazard map
Population density
Fuzzy logic
Settlements

1. Introduction

Important legal regulations and very expensive measures have been implemented since the early 2000s to reduce the effects of disasters and emergencies in Turkey (Tüney 2015). However, the desired result has not been reached yet. Despite measures being taken in disasters originating from geological, climatic, biological, technological, and social reasons, negative consequences continue to be encountered (President's Annual Program 2020). For this reason, it is aimed to obtain data including the whole country that will contribute to achieving the intended results.

Turkey is located in a geography that is affected by some of the sources of disaster and emergencies around the world less, and also some of them more (AFAD 2014). By combining the definitions given by Şahin (2013), Ergüney (2007), Özşahin (2013), Akıncı et al. (2010), Altun (2018), and Birinci and Yılmaz (2020), a comprehensive definition of disaster can be given as "Unavoidable, natural or human-induced, mass injury, and mass death, major loss of property or environmental damage". Disaster sources (and subgroup numbers) can be categorized into 4 main groups and 24 subgroups such as biological (4 subgroups including epidemic disease, insect invasion, animal invasion, and erosion), earthquake and water events (6 subgroups including earthquake, volcanic eruption, dry mass movement, crashes from space to earth, flood-flood and including wet mass movement), atmospheric and climatic events (7 subgroups including storm, rainfall, lightning strike, extreme cold, extreme heat, drought, and fire) and human-related incidents (7 subgroups including mining accidents, gun accidents, transportation accidents, fire,

* *Corresponding author*. Tel.: +90-362-312-1919 ; Fax: +90-362-457-6094 ; E-mail address: fbirinci@omu.edu.tr (F. Birinci)
ISSN: 2149-8024 / DOI: https://doi.org/10.20528/cjsmec.2023.02.002

war, terror, and mass migration). For an incident to be considered a disaster", there should consider some determining limit values such as at least 10 dead or 50 injured, become at least 100 people affected, effective in general life, historical value, and at least 20 hectares of burned area in case of a forest fire. No such preliminary assessment isn't made for an "emergency".

7628 people died in natural disasters and 411 million people were affected by disasters only in 2016 (Gökçe et al. 2008; Ersoy et al. 2017). The five major disasters and deaths that caused the most casualties in 2017 were in South Asia (flood) 2700, Iran and Mexico (earthquake) 999, Sierra Leone (landslide) 500, and Colombia (flood + landslide) 329, with a total death toll of 4498. (Erhan et al. 2018).

Considering all disasters in Turkey, it is seen that natural disasters have a distinct impact. In approximately 100 years after the beginning of the 20th century, in natural disasters such as earthquakes, landslides, floods, rock falls, and avalanches, 87000 people died, 210000 people were injured and 650654 buildings were destroyed or severely damaged (Ergüney 2007), in approximately 10 years after 1990, 19964 people died, 55802 people were injured, 1078200 people were left homeless, 19494300 people were affected by disasters, and an economic loss of 17.46 billion US dollars (average 1.74 billion $/year) are recorded (JICA 2004). On the other hand, Keleş (2002) gives the number of people who lost their lives as a result of natural disasters in Turkey between the years 1930-2020 as 100000 and the number of damaged houses as 600000. If the Elazig-Malatya earthquake (6.8 magnitudes, 41 dead), Izmir-Samos earthquake (6.6 magnitudes, 117 dead), and Van-Bahçesaray avalanche fall (42 dead) are added to these, the importance that should be given to disasters and emergencies in Turkey emerges. In the avalanche incident in Van, 5 of the 7 first people who were under the avalanche died. In the comprehensive intervention to save the remaining 2 people, when there is an avalanche blasted again, 35 more people from the rescue team died. The absence of any means of communication at the scene increased the death toll.

Considering the case studies in the form of very short notes presented above in the world and Turkey, it is understood that more comprehensive studies and a data repository are needed to develop extensive planning and applicable projects for disasters and emergencies. Experience has shown that 75% of survivors survive when rescue and debris removal efforts are initiated 30 minutes after the disaster (Dedeoğlu 2017; Erkal and Değerliyurt 2013), 95% of the cases in the centers in the first 10 minutes, 97% of the rural cases are reached within 30 minutes. Although the 20-30 minutes access time is considered reasonable for disasters, it should be taken into account that this time is too long in emergencies. Today there are many polymer-based materials in workplaces and vehicle manufacturing. In environments with polymer-based materials, the spread of the fire to the whole environment takes place in the order of 2-3 minutes. Therefore, it should be aimed to reduce the response time to emergencies due to burning in workplaces and vehicles to much less than 10 minutes.

For this purpose, in this study, a disaster and emergency profile have been tried to be created from the data prepared by taking the current situation in Turkey into consideration to be used in disaster and emergency preparation studies. It has been tried to determine how it will be possible to respond quickly in disaster and emergency situations with sufficient trained and equipped core teams. It has developed suggestions about efforts to obtain results that would minimize access time.

2. Methodology

Turkey is between 26-45 East and 36-42 North latitudes. In Turkey, there are 81 provinces (30 metropolitan cities, 51 cities), 828.88 districts belonging to these cities, metropolitan cities, and 50305 neighborhoods or villages belonging to these metropolitan cities, cities, and districts. At the beginning of 2021 (31 December 2020-01 January 2021), its population is 83614362 (TÜİK 2021) and its acreage is 780040 km2. All compiled or calculated data were collected in 43 columns and 50305 rows. The transportation speed values of the settlements to the districts and provincial centers to which they are connected were calculated simply from the distance and time information (speed = road/time). Approximate area values of the neighborhoods and villages were calculated by dividing the district area by the number of settlements and assuming equal (this data is not available collectively in any institution). Population density is approximately calculated from population and area information (density = population/area). Area values of districts and provinces were taken directly (HGM 2021), and population densities were calculated.

The earthquake hazard map parameters are approximately determined by using fuzzy logic according to the latitudes and longitudes of the settlements from the published parameters (AFAD 2018), which are not related to residential areas, calculated with equal spacing and equal increment. Parameters in the project design are determined according to the coordinates of the land where the building will be built. Published or calculated values are not available as project data. The approximate values calculated here belong to a coordinate belonging to the center of the settlements and were determined only for evaluation in the analysis of the data. Very few were calculated as R>0.85, and most were calculated as close to R>0.95 and were used. Considering the geographical features, meteorological characteristics, altitudes, and earthquake risks of the settlements, "similar regions" were determined (this is zoning specific to the study). Similar regions were specially designed for this study according to the color intensity from the earthquake hazard map, with latitude and longitude being integers. Similar regions are given in Fig. 1(a) and "geographical regions" are given in Fig. 1(b).

Since the "Earthquake Hazard Map" used in Turkey before 2018 is in many publications and official documents, Fig. 2(a) shows the "Earthquake Hazard Map (Parameters)", then it was developed using more advanced methods after 2018 and started to be used since 2020 shown in Fig. 2(b). Selected settlements (province, dis-

trict, town, neighborhood, and village) in the same geography are shown in Fig. 2(c) to make a comparison for the parameters to be used in the design phase with both maps. The locations, earthquake zone numbers, and earthquake hazard map parameters of the settlements selected for comparison are given in Table 1.

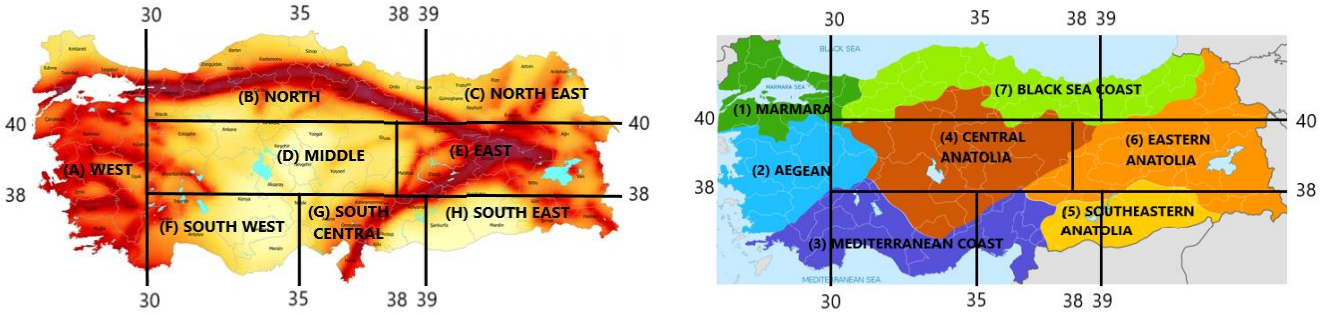

(a) (b)

Fig. 1. Similar and geographical regions: a) Similar regions (8 pieces); b) Geographical regions (7 pieces).

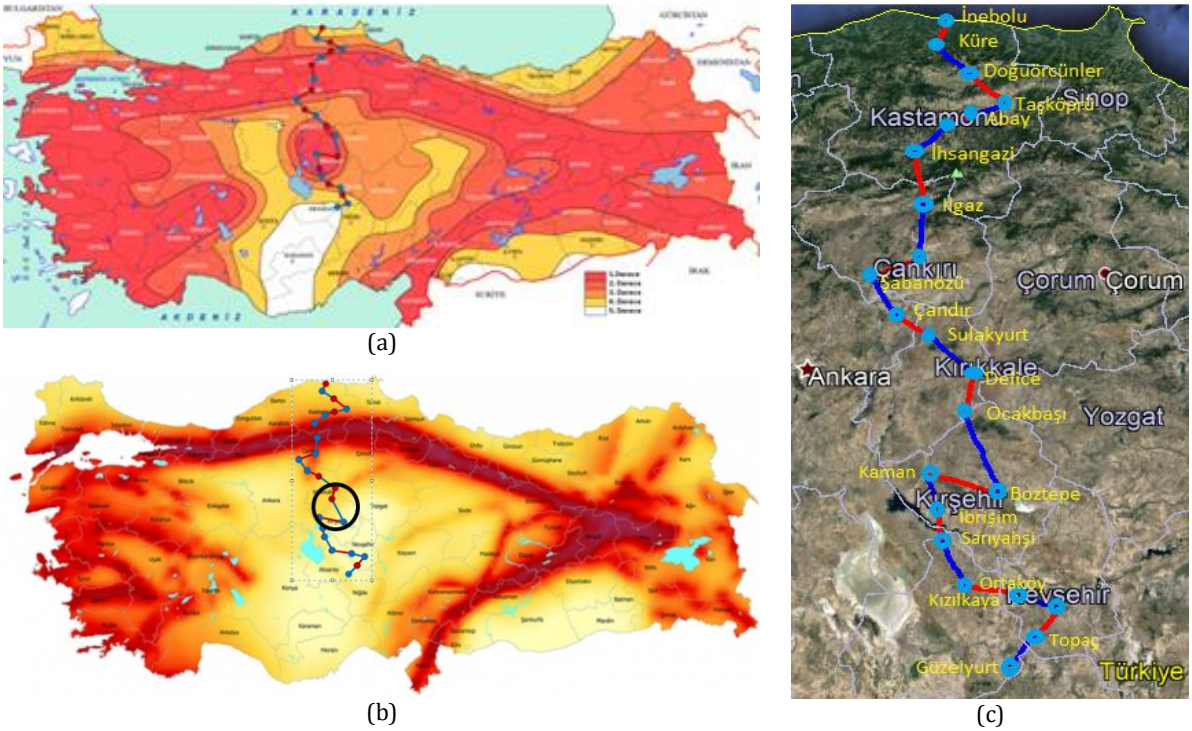

(a) (b) (c)

Fig. 2. Earthquake map before and after 2018 in Turkey: a) Turkey earthquake zones map (Özmen, 2012); b) Turkey earthquake hazard map (AFAD, 2018); c) Compared geography.

Spectral acceleration S_S - 475 was chosen since the design is thought to be based on a design spectrum, 10% probability of being exceeded in 50 years. *ZC* was chosen as an average soil class from the old earthquake code to include soil properties. In the new earthquake regulation, $S_{DS}=S_S*F_S=S_S$x1.3 was used, taking into account the 30% magnification factor in which S_{DS} and F_S refer to the spectral acceleration coefficient and soil effect coefficient, respectively. In order to be able to make a comparison along the entire line (Fig. 2(c)), by considering I=1 for the formula $A(T)= A_0*I*S(T)$ in DBYBHY (2007), $S(T)$=2.5 is taken from the acceleration spectrum curve for the earthquake with 10% probability of being exceeded in 50 years and acceleration spectrum coefficients were determined as A_0*2.5 (Table 1). The comparison of the obtained design earthquake parameters is given in Fig. 3, the longitudinal section of the line with the compared settlements, and the map views corresponding to this longitudinal section in both old (before 2018) and new (after 2018) earthquake hazard maps are given in Fig. 4. While the earthquake zones between Delice and Ortaköy (the area in the east and north-east of Salina) on the line examined change as 2, 1, 3 in the old earthquake zones map, they are seen as low, medium, and low risk in the new earthquake hazard map (Fig. 2(a-b)).

3. Application and Results

After the compiled or calculated values of each settlement are placed in the table, they are determined separately according to the districts and provinces, according to each option of distance, transportation time, and

transportation speed, according to the number of earthquake zones (EQ+) and without taking into account earthquake zones (EQ-), the number of settlements in Turkey in general, similar regions and geographical regions corresponding to the limit values, living population, and settlement areas are calculated on the tables. Calculation steps and distance, time, speed, altitude, and earthquake zone range values are shown in Fig. 5, and the interval values determined for the earthquake hazard map parameters are given in Table 2.

The number of settlements, areas, and populations of similar regions, geographical regions, and settlements, which are calculated for Turkey in general, are given in Tables 3 and 4.

Turkey's average values of all data; according to the district center; distance: 17.79 km, transportation time: 23.94 minutes, transportation speed: 42.04 km/h, depending on the city center; distance: 64.15 km, travel time: 62.85 minutes, travel speed: 57.78 km/h are found. The average altitude of settlements is 828.88 m. In practice, it is thought that it would be more appropriate to use distances as planning data rather than transportation speed and times to city and district centers because the actual values differ.

Table 1. Comparison of old and new earthquake data.

Settlement unit (city, district, neighborhood/village)	Intermediate distance (km)	Distance to start (km)	Earthquake zone number	Old regulation, A_0*S(T)= A_0*2.5	New regulation, S_S-475*1.3	Latitude	Longitude
İNEBOLU/ KASTAMONU	0	0	4	0.25	0.507	41.978799	33.759147
KÜRE/KASTAMONU	23	23	3	0.50	0.562	41.804781	33.712784
DOĞUÖRCÜNLER/DEVREKANİ/KASTAMONU	28	51	3	0.50	0.607	41.673763	33.943993
TAŞKÖPRÜ/KASTAMONU	28	79	2	0.75	0.562	41.804781	33.712784
ABAY/TAŞKÖPRÜ/ KASTAMONU	23	102	2	0.75	0.809	41.438261	33.987094
KASTAMONU	24	126	1	1.00	0.904	41.367804	33.769450
İHSANGAZİ/KASTAMONU	30	156	1	1.00	1.278	41.203793	33.554760
ILGAZ/ÇANKIRI	32	188	1	1.00	1.936	40.925326	33.627021
ÇANKIRI	38	226	1	1.00	0.907	40.595661	33.613251
ŞABANÖZÜ/ÇANKIRI	33	259	2	0.75	0.879	40.473757	33.278431
ÇANDIR/KALECİK/ANKARA	32	291	3	0.50	0.796	40.257377	33.467243
SULAKYURT/KIRIKKALE	28	319	3	0.50	0.581	40.157698	33.717195
DELİCE/KIRIKKALE	38	357	2	0.75	0.623	39.943350	34.032498
OCAKBAŞI/DELİCE/KIRIKKALE	23	380	2	0.75	0.572	39.750543	33.995350
BOZTEPE/KIRŞEHİR	24	404	1	1.00	0.268	39.270311	34.265943
KAMAN/KIRŞEHİR	32	436	1	1.00	0.511	39.358468	33.723322
İBRİŞİM/KAMAN/KIRŞEHİR	23	459	1	1.00	0.350	39.175461	33.820492
SARIYAHŞİ/AKSARAY	30	489	2	0.75	0.317	38.979569	33.836312
ORTAKÖY/AKSARAY	32	521	3	0.50	0.285	38.736610	34.039259
KIZILKAYA/GÜLŞEHİR/ NEVŞEHİR	38	559	3	0.50	0.242	38.698141	34.420738
NEVŞEHİR	28	587	4	0.25	0.270	38.625088	34.719940
TOPAÇ/ACIGÖL/NEVŞEHİR	23	610	4	0.25	0.273	38.473841	34.558962
GÜZELYURT/AKSARAY	35	645	5	0.00	0.354	38.276798	34.369992
TOTAL	645						

Note: The values A_0 are corresponding to the DBYBHY, Table 2.4 (2007)

Table 2. Specified ranges for earthquake hazard map parameters (TBDY 2018).

*	PGA 2475	PGA 475	PGA 72	PGA 43	S_S - 2475	S_S - 475	S_S - 72	S_S - 43
1	PGA>1	PGA>0.75	PGA>0.3	PGA>1	S_S>3	S_S >1.8	S_S>0.75	S_S>0.4
2	0.75<PGA≤1	0.5<PGA≤0.75	0.225<PGA≤0.3	0.75<PGA≤1	2.25<SS≤3	1.35<S_S≤1.8	0.5<S_S≤0.75	0.3<S_S≤0.4
3	0.5<PGA≤0.75	0.25<PGA≤0.5	0.15<PGA≤0.225	0.5<PGA≤0.75	1.5<S_S≤2.25	0.9<S_S≤1.35	0.25<S_S≤0.5	0.2<S_S≤0.3
4	0.25<PGA≤0.50	0.125<PGA≤0.25	0.075<PGA≤0.150	0.25<PGA≤0.50	0.75<SS≤1.50	0.45<S_S≤0.9	0.125<S_S≤0.25	0.1<S_S≤0.2
5	PGA≤0.25	PGA≤0.125	PGA≤0.075	PGA≤0.25	S_S≤0.75	S_S≤0.45	S_S≤0.125	S_S≤0.1
*	S_1 - 2475	S_1 - 475	S_1 - 72	S_1 - 43	PGV 43	PGV 72	PGV 475	PGV 2475
1	S_1>0.8	S_1>0.4	S_1>0.19	S_1>0.1	PGV>10	PGV>18	PGV>60	PGV>100
2	0.6<S_1≤0.8	0.3<S_1≤0.4	0.135<S_1≤0.18	0.075<S_1≤0.1	7.5<PGV≤10	13.5<PGV≤18	45<PGV≤60	75<PGV≤100
3	0.4<S_1≤0.6	0.2<S_1≤0.3	0.09<S_1≤0.135	0.05<S_1≤0.075	5<PGV≤7.5	9<PGV≤13.5	30<PGV≤45	50<PGV≤75
4	0.2<S_1≤0.4	0.1<S_1≤0.2	0.045<S_1≤0.09	0.025<S_1≤0.05	2.5<PGV≤5	4.5<PGV≤9	15<PGV≤30	25<PGV≤50
5	S_1≤0.2	S_1≤0.1	S_1≤0.045	S_1≤0.025	PGV≤2.5	PGV≤4.5	PGV15	PGV≤25

*Sequence, earthquake zone number

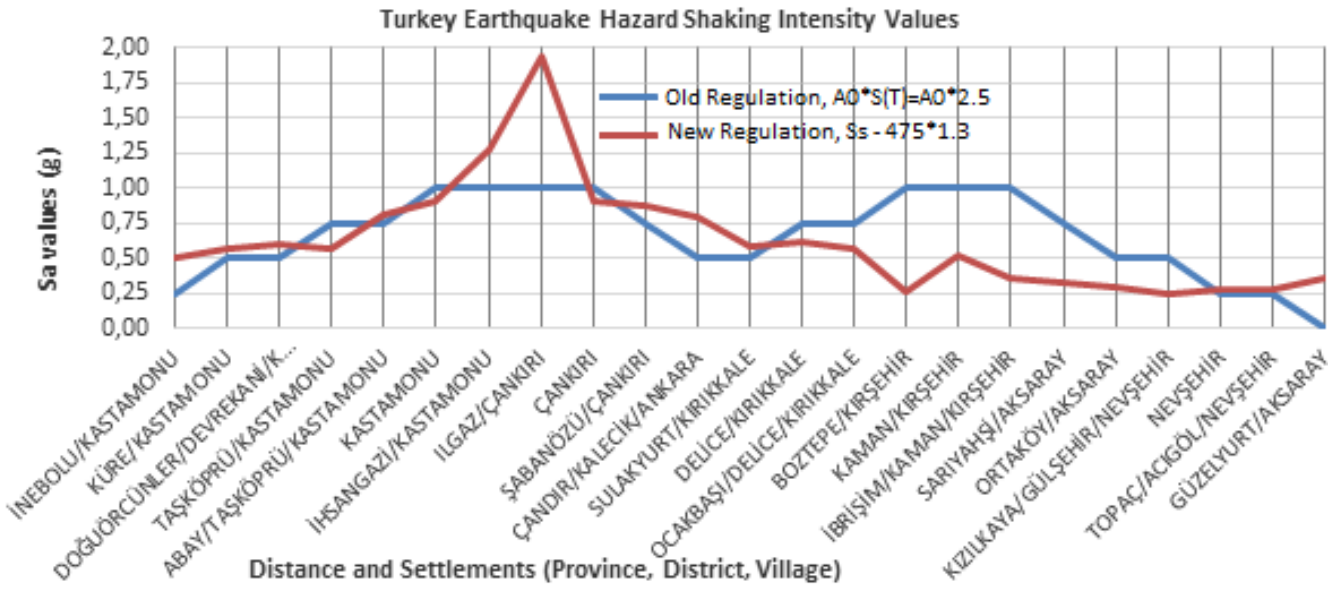

Fig. 3. Comparison of earthquake data before and after 2018 in Turkey.

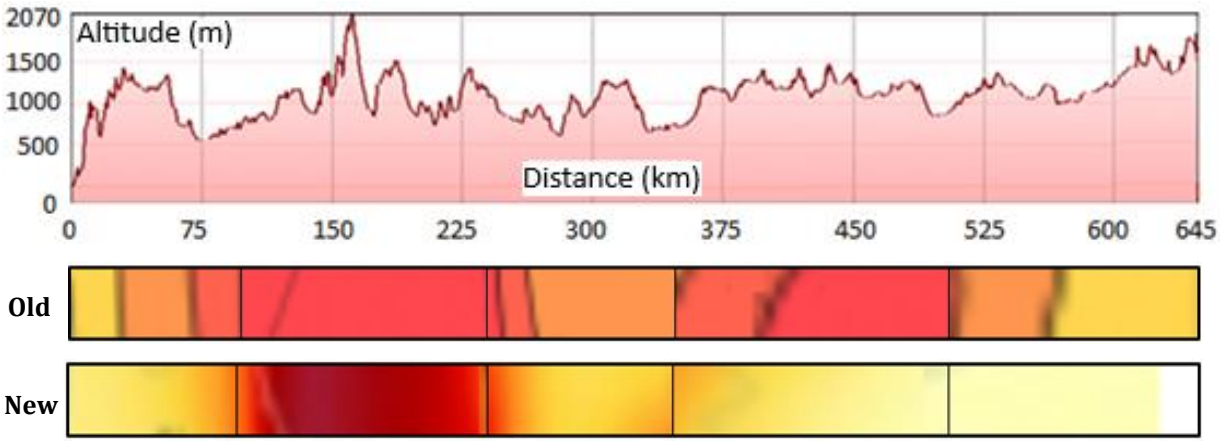

Fig. 4. Settlements longitudinal section and their situations in the old and new earthquake map.

Table 2. Specified ranges for earthquake hazard map parameters (TBDY 2018).

*	PGA 2475	PGA 475	PGA 72	PGA 43	S_S - 2475	S_S - 475	S_S - 72	S_S - 43
1	PGA>1	PGA>0.75	PGA>0.3	PGA>1	S_S>3	S_S >1.8	S_S>0.75	S_S>0.4
2	0.75<PGA≤1	0.5<PGA≤0.75	0.225<PGA≤0.3	0.75<PGA≤1	2.25<SS≤3	1.35<S_S≤1.8	0.5<S_S≤0.75	0.3<S_S≤0.4
3	0.5<PGA≤0.75	0.25<PGA≤0.5	0.15<PGA≤0.225	0.5<PGA≤0.75	1.5<S_S≤2.25	0.9<S_S≤1.35	0.25<S_S≤0.5	0.2<S_S≤0.3
4	0.25<PGA≤0.50	0.125<PGA≤0.25	0.075<PGA≤0.150	0.25<PGA≤0.50	0.75<SS≤1.50	0.45<S_S≤0.9	0.125<S_S≤0.25	0.1<S_S≤0.2
5	PGA≤0.25	PGA≤0.125	PGA≤0.075	PGA≤0.25	S_S≤0.75	S_S≤0.45	S_S≤0.125	S_S≤0.1
*	S_1 - 2475	S_1 - 475	S_1 - 72	S_1 - 43	PGV 43	PGV 72	PGV 475	PGV 2475
1	S_1>0.8	S_1>0.4	S_1>0.19	S_1>0.1	PGV>10	PGV>18	PGV>60	PGV>100
2	0.6<S_1≤0.8	0.3<S_1≤0.4	0.135<S_1≤0.18	0.075<S_1≤0.1	7.5<PGV≤10	13.5<PGV≤18	45<PGV≤60	75<PGV≤100
3	0.4<S_1≤0.6	0.2<S_1≤0.3	0.09<S_1≤0.135	0.05<S_1≤0.075	5<PGV≤7.5	9<PGV≤13.5	30<PGV≤45	50<PGV≤75
4	0.2<S_1≤0.4	0.1<S_1≤0.2	0.045<S_1≤0.09	0.025<S_1≤0.05	2.5<PGV≤5	4.5<PGV≤9	15<PGV≤30	25<PGV≤50
5	S_1≤0.2	S_1≤0.1	S_1≤0.045	S_1≤0.025	PGV≤2.5	PGV≤4.5	PGV15	PGV≤25

*Sequence, earthquake zone number

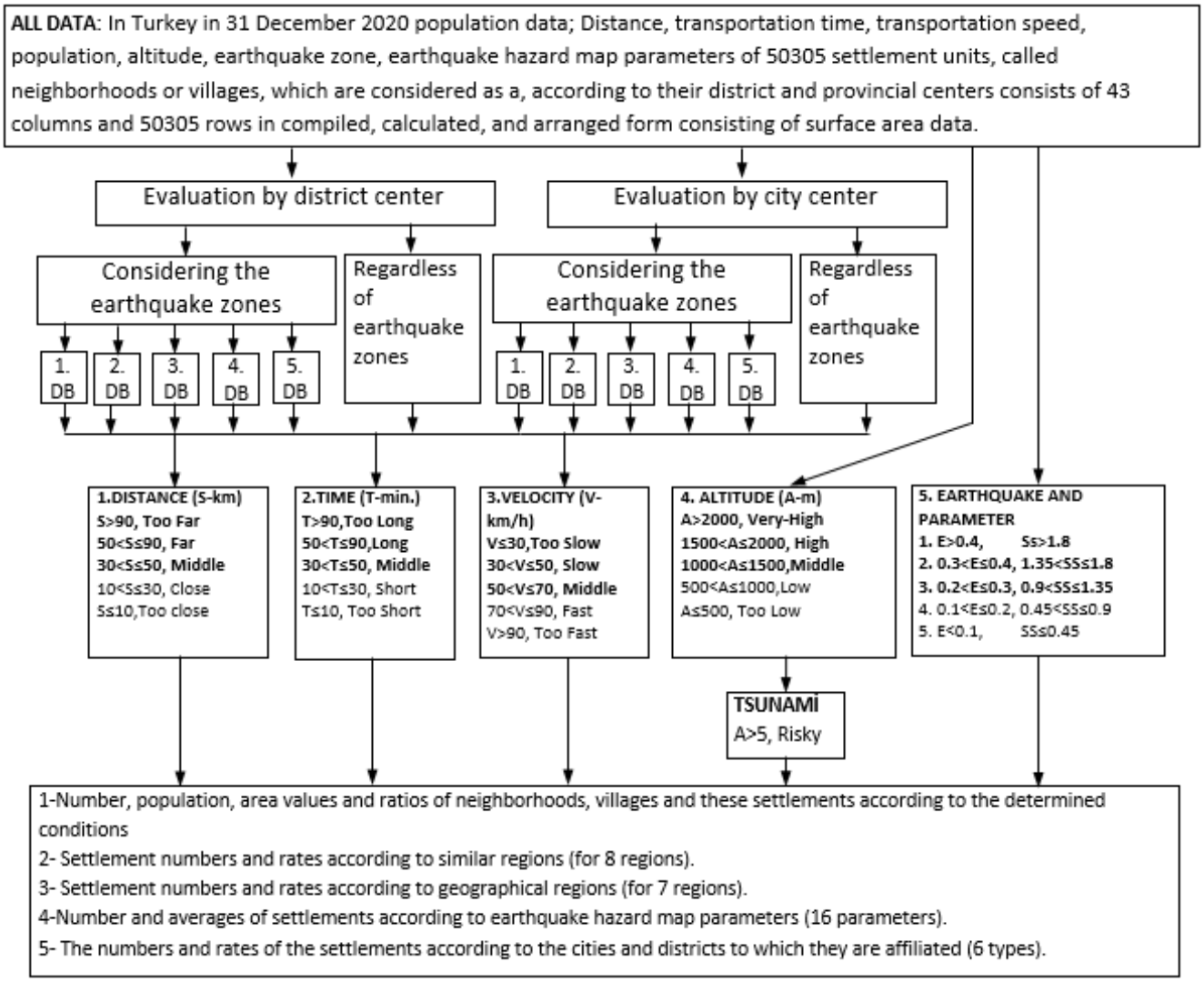

Fig. 5. Data and spreadsheet formatting.

According to similar regions in Tables 3 and 4, the number of settlements is highest in the North (11585 people), the largest area (157292.93 km^2, in the Middle), and the highest population in the West (34097535 people) takes place. According to geographical regions, the number of settlements takes place the highest in the Black Sea (11221), the largest area in Central Anatolia (192328.10 km^2), and the highest population in Marmara (25377324 people). According to the state of the district to which the settlements are connected, the highest number of settlements (20392), the largest area (343879.00 km^2), and the highest population (37214062 people) is found in the settlements defined as "MD: Metropolitan District".

Table 3. Number, area, and population of settlements in similar regions and geographical regions.

Similar regions					Geographical regions				
Code	Nomenclature	Number	Area*	Populations	Code	Nomenclature	Number	Area	Populations
(A)	West	10652	140353.87	34097535	(1)	Marmara	6074	66746.42	25377324
(B)	North	11585	126147.41	8950081	(2)	Aegean	6189	89478.70	10689115
(C)	North East	3624	54365.13	2154723	(3)	Mediterranean	4885	89671.16	10759218
(D)	Middle	7197	157292.93	11449973	(4)	Central Anatolia	8604	192328.10	13691779
(E)	East	6882	122769.21	5926494	(5)	Southeastern Anatolia	5862	76151.20	9118921
(F)	South West	3152	77251.04	7095001	(6)	Eastern Anatolia	7470	149157.80	6061837
(G)	South Central	4486	53657.05	9518321	(7)	Black Sea	11221	116506.60	7916168
(H)	South East	2727	48203.36	4422234					
Top three totals		29434	423794.21	55065829			27295	457992.50	49828321
TOTAL		50305	780040	83614362			50305	780040	83614362

Note: * The values complied from the Republic of Turkey Ministry of Natural Defense General Directorate of Mapping (2021).

Table 4. Distribution, number, area, and population of settlements by district and province types.

The city status to which the neighborhoods and villages are affiliated (numbers and proportions)							
Code	Nomenclature	Number	Ratio, %	Area	Ratio, %	Population	Ratio, %
MCD	Metropolitan Central District	5470	10.87	55391.00	7.10	27942170	33.42
MD	Metropolitan District	20392	40.54	343879.00	44.08	37214062	44.51
CCD	City Center District	1900	3.78	25681.58	3.29	7677970	9.18
CCDV	City Center District Village	3570	7.10	49969.00	6.41	1262423	1.51
CD	City District	4247	8.44	68300.71	8.76	5718451	6.84
CDV	City District Village	14726	29.27	236818.71	30.36	3799286	4.54
First three sum		40588	80.68	648998.42	83.20	72834202	87.11
TOTAL		50305	100.00	780040	100.00	83614362	100.00

The distance to the district center to which each settlement is connected, according to each option of the distance, travel time, and transportation speed (first three cases from "middle" to the most negative, shown in Fig. 5), according to the earthquake zone numbers (EQ+) and earthquake zones. (EQ-), corresponding to the limit values, the number of settlements in similar regions and geographical regions, the number of living population, settlement areas, their location (explained in Tables 3 and 4), and their rates according to Turkey overall (%) are given in Table 5. The results obtained by making the same process according to the provincial centers are given in Table 6.

According to the evaluation according to the district center, it is seen that EQ-: 8495 (EQ+: 7337, 14.59%) of the settlements (16.89%) are located more than 30 km away, they have an area of 163442 km2 (20.95%) and 5604523 people live in this area (6.70%). It is seen that the number of settlements where the transportation time is more than 30 minutes is 28.69%, the area is 31.98% and the population is 12.70%, the number of settlements where the transportation speed is less than 50 km/h is 97.45%, the area is 96.53% and the population is 98.75%.

In similar regions more than 30 km away from the district center, the highest number of settlements are in the East (1722 units), according to geographical regions in Eastern Anatolia (1903 units), and according to the city type, the most are in the Metropolitan District Center (3231units). The highest number of settlements in similar regions longer than 30 minutes are located in the East (3013 units), according to geographical regions in Eastern Anatolia (3165 units), and according to the city type, most are in the Metropolitan District Center (5583 units). It is seen that the number of settlements where the transportation speed is less than 50 km/h the most settlements are in the North (11403 units), according to geographical regions, it is seen in Eastern Anatolia (11098 units), according to the city type, it is mostly in the Metropolitan District Center (19902 units).

According to the evaluation according to the city center, it is seen that 38314 of the settlements (76.16%) are located more than 30 km away, they have an area of 648241 km2 (83.10%) and 34680977 people live in this area (41.48%). It is seen that the number of settlements where the transportation time is more than 30 minutes is 79.54%, the area is 85.50% and the population is 46.82%, the number of settlements where the transportation speed is less than 50 km/h is 94.54%, the area is 96.23% and the population is 81.63%.

In similar regions more than 30 km away from the city center, the highest number of settlements are located in the North (8996 units), according to geographical regions in the Black Sea (8442 units), and according to the city type, the most are in the City District Village (18452 units). The highest number of settlements in similar regions longer than 30 minutes are located in the North (8628 units), according to geographical regions in the Black Sea (8986 units), and according to the city type, most are located in the Metropolitan District (18803). It is seen that the number of settlements where the transportation speed is less than 50 km/h the most settlements are in the North (11106 units), according to geographical regions, it is seen in the Black Sea (8423 units), according to the city type, it is mostly in the Metropolitan District (20179 units).

The altitudes of each settlement, earthquake zone numbers, and each option of the earthquake hazard map parameters (the first three cases, from "middle" to the most negative, shown in Fig. 5), according to the earthquake zone numbers (EQ+) and without considering the earthquake zones (EQ-), corresponding to the determined limit values, the number of settlements in similar regions and geographical regions, living population, settlement areas, location (explained in Table 3 and Table 4), their rates (%) and altitude compared to overall Turkey, tsunami risk assessment (ratios not given) findings for settlements with A> 5 are given in Table 7. The tsunami risk of Turkey is given as 4.71 m for the Mediterranean, including the Aegean Sea, depending on the fault movement (the time to reach the shore in 8 minutes, the advancement distance is 50 m) and 3 m for the Black Sea (BDTİM, 2017). For this reason, the altitude value to include both situations was determined as 5 m.

When the altitudes are evaluated, 19122 (38.01%) settlements are located at an elevation of more than 1000 m, 26757 (53.19%) settlements exist in 1., 2. or 3. earthquake zones (earthquake hazard map parameters have been evaluated separately) and it is seen that 49623348 people (59.35%) live in these settlements. According to the evaluation made for the medium-high risk zone, 26483 (52.64%) settlements are located in an area of 382395 km2 (49.02%) and 49623348 people (59.35%) live in this area.

Table 5. Evaluation results of distance, transportation time, and transportation speed data according to the district center.

		Evaluation according to the district center								
		Distance >30 km	Location	%	Duration >30 min	Location	%	Speed <50 km/h	Location	%
Number of settlements (neighborhood-village)	EQ+	7337	-	14.59	12475	-	24.80	42589	-	84.66
	EQ-	8495	-	16.89	14435	-	28.69	49020	-	97.45
Area of settlements (km²)	EQ+	135353	-	17.35	211582	-	27.12	641453	-	82.23
	EQ-	163442	-	20.95	249481	-	31.98	752965	-	96.53
Living population (person)	EQ+	4212404	-	5.04	8108594	-	9.70	71344012	-	85.33
	EQ-	5604523	-	6.70	10619290	-	12.70	82568950	-	98.75
Number of settlements and region (maximum) in a similar region	EQ+	1722	(E)	3.42	2894	(E)	5.75	10429	(B)	20.73
	EQ-	1722	(E)	3.42	3008	(B)	5.98	11403	(B)	22.67
Settlement in a similar region number and region (2nd most)	EQ+	1280	(B)	2.54	2675	(B)	5.32	10122	(A)	20.12
	EQ-	1456	(D)	2.89	2894	(E)	5.75	10502	(A)	20.88
Number of settlements in similar regions and regions (3rd most)	EQ+	1118	(A)	2.22	2138	(A)	4.25	6700	(E)	13.32
	EQ-	1386	(B)	2.76	2172	(A)	4.32	6731	(D)	13.38
Number of settlements in the geographical region and region (most)	EQ+	1903	(6)	3.78	3165	(6)	6.29	8756	(7)	17.41
	EQ-	1903	(6)	3.78	3185	(7)	6.33	11098	(7)	22.06
Number of settlements in the geographical area and region (2nd most)	EQ+	1245	(7)	2.47	2559	(7)	5.09	7248	(6)	14.41
	EQ-	1827	(4)	3.63	3165	(6)	6.29	8087	(4)	16.08
Settlement in the geographical region number and region (3rd most)	EQ+	1206	(5)	2.40	1840	(5)	3.66	6054	(2)	12.03
	EQ-	1414	(7)	2.81	2302	(4)	4.58	7248	(6)	14.41
Number of settlements and city type by city type (most)	EQ+	2673	MD	5.31	4720	MD	9.38	17170	MD	34.13
	EQ-	3231	MD	6.42	5583	MD	11.10	19902	MD	39.56
Number of settlements and city type by city type (2nd most)	EQ+	2635	CDV	5.24	4523	CDV	8.99	12569	CDV	24.99
	EQ-	2895	CDV	5.75	5079	CDV	10.10	14257	CDV	28.34
Number of settlements and city type by city type (3rd most)	EQ+	914	MCD	1.82	1502	MCD	2.99	4679	MCD	9.30
	EQ-	1073	MCD	2.13	1790	MCD	3.56	5362	MCD	10.66

From the altitude assessment, it is seen that 411010 people live in 148 settlements in an area of 1895.77 km2 with an altitude of 5 m or less. According to similar regions, 55 of them are located in the West, while 63 according to geographical regions are in the Mediterranean. 118 of the 148 settlements are also located in settlements affiliated with Metropolitan District.

Limit values determined for earthquake hazard map parameters are given in Fig. 5. The values in Table 8 are calculated according to the ranges given in Table 2 and determined by 5 limit values obtained by dividing into 4 parts between the maximum and minimum values in Turkey. Since Turkey earthquake hazard map parameters were determined for locations that have equal increments of latitudes and longitudes in general, they do not correspond every time to settlements. For this reason, both the maximum and minimum values of Turkey in general and the maximum, minimum, and average values of the settlements are given together in the table. Here, as shown in Fig. 5, from "middle" to negative, the first three cases where the earthquake zone degree is less than 3 (3rd, 2nd, 1st-degree earthquake zone) are taken into consideration.

The maximum value of the design earthquake S_S - 475 according to the settlements is 2.001, the minimum value is 0.137 and the average value is 0.717. The number of settlements where the S_S - 475 value is greater than 0.9 (approximately the same whether the earthquake zone is taken into account or not) is 13292. It has been observed that the area of these settlements is approximately 174380 km2 and the living population is 28321962 people.

4. Discussion and Recommendations: Sampling for Turkey-Trabzon-Akçaabat

According to the findings obtained from the study, it is understood that intervention in disasters and emergencies from the central point cannot be as fast as neces-

sary. For this reason, it was concluded that a solution can be produced by establishing “core monitoring and response centers (CMICEN)” consisting of 2-4 people trained for possible disasters and emergencies for a quick solution. The recommended centers should be formed primarily from volunteers, and the necessary training should be provided for this team. Under the leadership of AFAD (DEMP-Disaster and Emergency Management Presidency), preparations and training programs are already provided voluntarily. Providing the necessary equipment for the team’s immediate response to be determined at the local level, evaluating if available volunteers, and providing uninterrupted communication opportunities for the team at all times must be provided. The communication cycle of "public-112 Emergency Service- CMICEN (ÇEKMER)" is important for this. For areas where existing communication tools are not available, it is necessary to provide the opportunity to communicate immediately. The use of satellite-connected communication tools and radio equipment should also be considered as an alternative. For the success of the aforementioned studies, the condition that the volunteers permanently reside in the settlement where the center is established and that the public has access to these people together with the 112 Emergency Service should be observed.

Table 6. Evaluation results of distance, transportation time, and transportation speed data according to the city center.

		Evaluation according to the district center								
		Distance >30 km	Location	%	Duration >30 min	Location	%	Speed <50 km/h	Location	%
Number of settlements (neighborhood-village)	EQ+	33320	-	66.24	34849	-	69.28	41322	-	82.14
	EQ-	38314	-	76.16	40015	-	79.54	47559	-	94.54
Area of settlements (km²)	EQ+	550468	-	70.57	567585	-	72.76	639331	-	81.96
	EQ-	648241	-	83.10	666913	-	85.50	750621	-	96.23
Living population (person)	EQ+	30843316	-	36.89	34897644	-	41.74	58826414	-	70.35
	EQ-	34680977	-	41.48	39148967	-	46.82	68252597	-	81.63
Number of settlements and region (maximum) in a similar region	EQ+	8230	(B)	16.36	8628	(B)	17.15	10146	(B)	20.17
	EQ-	8936	(B)	17.76	9379	(B)	18.64	11092	(B)	22.05
Settlement in a similar region number and region (2nd most)	EQ+	7692	(A)	15.29	8002	(A)	15.91	9646	(A)	19.18
	EQ-	8003	(A)	15.91	8312	(A)	16.52	10014	(A)	19.91
Number of settlements in similar regions and regions (3rd most)	EQ+	5524	(E)	10.98	5783	(E)	11.50	6662	(E)	13.24
	EQ-	5524	(E)	10.98	5783	(E)	11.50	6833	(D)	13.58
Number of settlements in the geographical region and region (most)	EQ+	6767	(7)	13.45	7189	(7)	14.29	8423	(7)	16.74
	EQ-	8442	(7)	16.78	8986	(7)	17.86	10636	(7)	21.14
Number of settlements in the geographical area and region (2nd most)	EQ+	5885	(6)	11.70	6169	(6)	12.26	7174	(6)	14.26
	EQ-	6689	(4)	13.30	6771	(4)	13.46	8121	(4)	16.14
Settlement in the geographical region number and region (3rd most)	EQ+	4964	(4)	9.87	5003	(4)	9.95	5905	(2)	11.74
	EQ-	5885	MD	11.70	6169	(6)	12.26	7174	(6)	14.26
Number of settlements and city type by city type (most)	EQ+	15759	MD	31.33	16057	MD	31.92	17344	MD	34.48
	EQ-	18452	CDV	36.68	18803	MD	37.38	20179	MD	40.11
Number of settlements and city type by city type (2nd most)	EQ+	12169	CDV	24.19	12431	CDV	24.71	12943	CDV	25.73
	EQ-	13706	CD	27.25	14009	CDV	27.85	14673	CDV	29.17
Number of settlements and city type by city type (3rd most)	EQ+	3106	CD	6.17	3065	CD	6.09	3631	MCD	7.22
	EQ-	3571	CD	7.10	3519	CD	7.00	4205	CD	8.36

Settlements in the coastal cities of Turkey are generally located in large river valleys flowing from the land to the sea, on the edges of small streams that are directed perpendicular to this stream, or on the plains in mountainous geography between small rivers. In the Black Sea Region, this formation is in the form of large rivers flowing in the South-North direction (valley bottom line) and small streams in the vertical direction (perpendicular to the valley). The main mode of transportation is the highway and it is built right next to the largest river, parallel

to it and following the natural geographical structure. If these roads unite the provincial and district centers, they also have the standard of "state and provincial roads", while the curved roads with a 10-20 m curvature radius that are connected to them and provide access to settlements are of very low standard (village road, forest road). For this reason, besides not allowing fast transportation, it has very large slopes and very narrow sections. From this, it is concluded that central teams cannot respond to disasters and emergencies as soon as necessary. For these reasons, it has been suggested to find CMICEN. Below, the centers determined for the Akçaabat district of Trabzon province (Metropolitan) are sampled. Fig. 6 shows the five centers proposed for Akçaabat and the geographical location and areas of responsibility of the AK4 center. If these centers are established based on an on-site examination, where all conditions are evaluated, their number and location may change.

Table 7. Altitude, earthquake, and tsunami assessment results of settlements.

		Altitude, earthquake parameters, and tsunami assessment, Altitude, Ground, Earthquake, Tsunami							
		Altitude >1000 m	Location	%	Earthquake EQ=1, 2, 3	Location	%	Tsunami A<5 m	Location
Number of settlements (neighborhood-village)	EQ+	16864	-	33.52	26483	-	52.64	148	-
	EQ-	19122	-	38.01	26757	-	53.19		
Area of settlements (km²)	EQ+	326160	-	41.81	381785	-	48.94	1895.77	-
	EQ-	386888	-	49.60	387486	-	49.68		
Living population (person)	EQ+	12498796	-	14.95	49434238	-	59.12	411010	-
	EQ-	16564350	-	19.81	49623348	-	59.35		-
Number of settlements and region (maximum) in a similar region	EQ+	5571	(E)	11.07	9735	(A)	19.35	55	(A)
	EQ-	5571	(E)	11.07	9866	(A)	19.61		
Settlement in a similar region number and region (2nd most)	EQ+	4320	(D)	8.59	5829	(B)	11.59	36	(G)
	EQ-	5275	(D)	10.49	5853	(B)	11.64		
Number of settlements in similar regions and regions (3rd most)	EQ+	2827	(B)	5.62	5492	(E)	10.92	28	(B)
	EQ-	2915	(B)	5.79	5492	(E)	10.92		
Number of settlements in the geographical region and region (most)	EQ+	6811	(6)	13.54	5702	(2)	11.33	63	(3)
	EQ-	6811	(6)	13.54	5702	(2)	11.33		
Number of settlements in the geographical area and region (2nd most)	EQ+	4336	(4)	8.62	5675	(6)	11.28	31	(2)
	EQ-	6287	(4)	12.50	5675	(6)	11.28		
Settlement in the geographical region number and region (3rd most)	EQ+	2525	(7)	5.02	5271	(1)	10.48	27	(1)
	EQ-	2662	(7)	5.29	5402	(1)	10.74		
Number of settlements and city type by city type (most)	EQ+	7486	CDV	14.88	11327	MD	22.52	118	MD
	EQ-	7945	CDV	15.79	11368	MD	22.60		
Number of settlements and city type by city type (2nd most)	EQ+	4482	MD	8.91	7626	CDV	15.16	22	MCD
	EQ-	5420	MD	10.77	7798	CDV	15.50		
Number of settlements and city type by city type (3rd most)	EQ+	1769	CCDV	3.52	2576	MCD	5.12	5	CD
	EQ-	1952	CCDV	3.88	2577	MCD	5.12		

Akçaabat, which has 73 settlements (neighborhoods), is the largest district after Ortahisar, which is the city center, with a population of 127 331 people (surface area 385 km2) among 18 districts of Trabzon. The natural events that are likely to pose the most important disaster risk can be listed as floods, landslides, rock falls, avalanches on high altitudes, and fires in places with old-fashioned and collective housing. Sera Lake, which was formed in 1950 due to landslides, is located within the boundaries of Akçaabat, just like Uzungöl, which is located in Çaykara and formed between 1610 and 1620. Yıldız, Söğütlü, Kireçhane, Kavaklı, Darıca, Zeytinlik, Çatalzeytin, Akçakale, and Taşlıca Creeks in the district are important streams flowing in the South-North direction. There are settlements among other small streams that are perpendicular to these streams. State and provincial roads are generally parallel to the large and long ones of these streams such as Söğütlü Creek. The roads

that provide access to the settlements are located from these main roads to the settlements as East-West on the left coast and West-East on the right coast. To reach the settlements in use, it is necessary to reach the main road by the big stream and then to go to the centers.

The number of roads providing a direct connection between settlements is both very few and of very low quality. For this reason, five centers have been established for the Akçaabat district, which will provide geographical situation, location of roads, and ease of transportation. If these centers are established, transportation to all settlements will be possible in 20 minutes at the most. Otherwise, it may be possible for the central intervention teams to be located in Trabzon (city center), Akçaabat, or Düzköy (districts close to the sample area) to all settlements in the selected area only in hours.

Table 8. Evaluation results of earthquake hazard map parameters in settlements.

Probability of exceeding in 50 years		% 2	% 10	% 50	% 68	% 2	% 10	% 50	% 68
Earthquake Parameter		PGA 2475	PGA 475	PGA 72	PGA 43	S_S - 2475	S_S - 475	S_S - 72	S_S - 43
Turkey Earthquake Hazard Map Parameters	Max	1.354	0.811	0.356	0.208	3.439	2.005	0.845	0.468
	Min	0.130	0.061	0.016	0.010	0.297	0.134	0.035	0.021
	Mean	0.532	0.276	0.103	0.071	1.286	0.647	0.233	0.161
Settlements in Turkey	Max	1.352	0.811	0.355	0.207	3.439	2.001	0.845	0.468
	Min	0.131	0.064	0.018	0.010	0.302	0.137	0.054	0.023
	Mean	0.564	0.302	0.115	0.079	1.381	0.717	0.267	0.179
Earthquake Zone: 1, 2, 3 and Parameters		Limit value							
		PGA>0.5	PGA>0.25	PGA>0.15	PGA>0.08	S_S>1.5	S_S >0.9	S_S >0.25	S_S >0.2
… of settlements complying with the conditions	Average values	0.843	0.397	0.210	0.105	2.148	1.266	0.474	0.237
	Number	26483	28234	12074	17469	18930	13292	23209	18898
	Area	382394.74	408856.42	157620.79	234111.79	263975.98	174676.70	322342.82	251924.41
	Population	49434238	52408621	23350328	35451606	37404991	28321962	45207053	39086530
		Without taking into account the earthquake region							
… of settlements complying with the conditions	Average	0.862	0.579	0.251	0.151	2.521	1.496	0.578	0.337
	Number	26757	28491	12113	17531	18997	13329	23303	18969
	Area	388105.2749	413753.4404	158325.7157	235254.3355	265239.1294	175320.0918	324074.3981	253220.04
	Population	49623348	52589237	23370662	35487030	37440402	28334477	45306019	39164618

Probability of Exceeding in 50 Years		% 2	% 10	% 50	% 68	% 2	% 10	% 50	% 68
Earthquake Parameter		S_1 - 2475	S_1 - 475	S_1 - 72	S_1 - 43	PGV 43	PGV 72	PGV 475	PGV 2475
Turkey Earthquake Hazard Map Parameters	Max	1.009	0.536	0.205	0.109	10.724	21.156	69.306	120.156
	Min	0.096	0.047	0.013	0.007	0.649	1.122	3.912	8.07296
	Mean	0.348	0.179	0.067	0.047	4.113	5.935	16.118	31.3627
Settlements in Turkey	Max	0.987	0.513	0.182	0.106	10.723	19.422	60.596	104.941
	Min	0.097	0.047	0.018	0.013	0.941	1.423	4.439	8.271
	Mean	0.380	0.201	0.077	0.053	4.817	7.054	22.002	35.432
Earthquake Zone: 1, 2, 3 and Parameters		Limit value							
		S_1>0.4	S_1>0.2	S_1>0.09	S_1>0.05	PGV>5	PGV>10	PGV>30	PGV>50
… of settlements complying with the conditions	Average values	0.843	0.397	0.210	0.105	2.148	1.266	0.474	0.237
	Number	19905	21659	15577	26824	21970	11171	8309	7572
	Area	262121.22	287961.62	199514.17	373445.56	292175.98	131751.06	97495.33	90831.36
	Population	41283061	43246858	35263434	47798524	42622483	26796006	18877263	14384817
		Without taking into account the earthquake region							
… of settlements complying with the conditions	Average	0.862	0.579	0.251	0.151	2.521	1.496	0.578	0.337
	Number	19992	21755	15655	26972	22069	11246	8364	7629
	Area	263711.49	289726.84	200925.51	376263.89	294015.81	133120.14	98472.78	91850.25
	Population	41381753	43356035	35349910	47946343	42733727	26874339	18897017	14405522

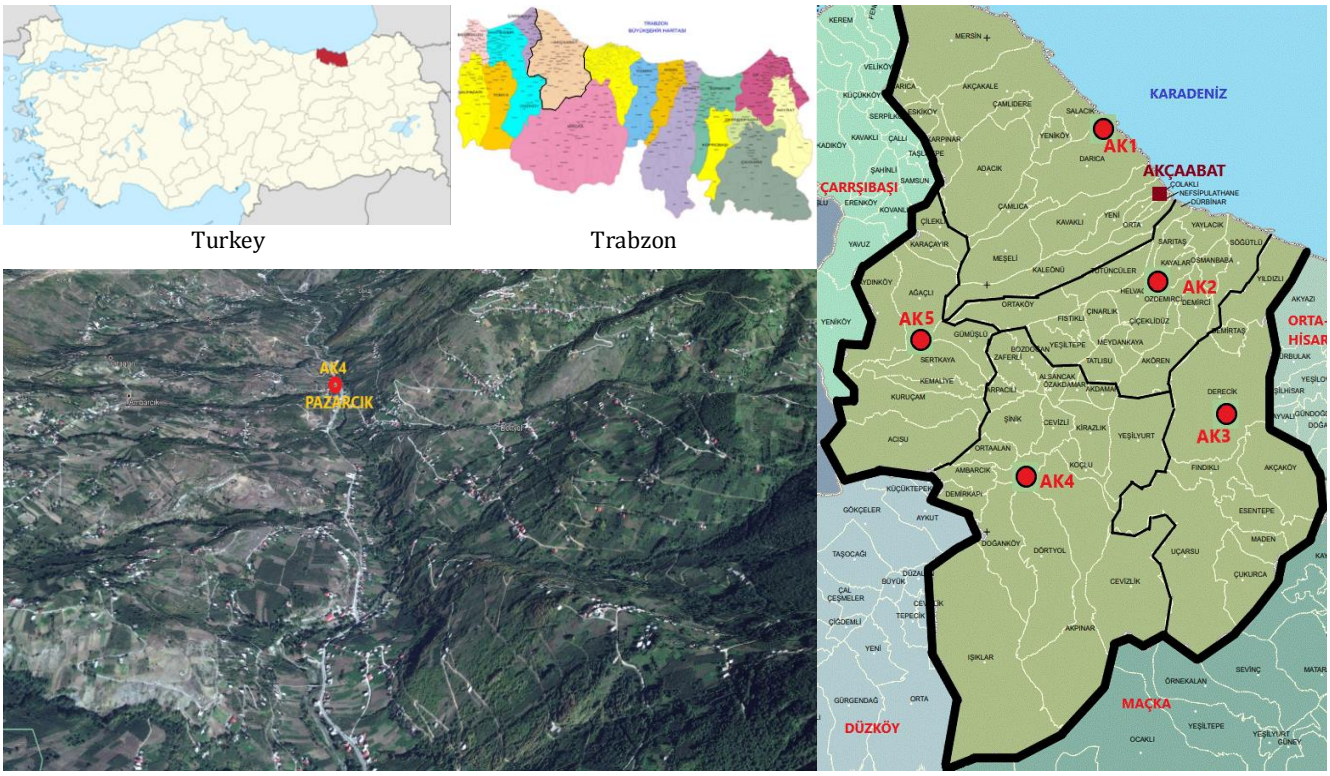

Fig. 6. Core monitoring and response centers-CMICEN sampling for Trabzon-Akçaabat.

5. Conclusions

For all disasters and emergencies caused by biological, earth-crust, and water events, atmospheric and climatic events, and human-related events, the distances of the place of disaster to the centers or intervention points, transportation times and speeds, and the altitudes of these places have a significant effect. In this study, settlements are approximately 18 km away, transportation time is approximately 23 minutes and transportation speed is at the level of 43 km/h according to Turkey and district centers. According to the provincial centers, the average distance is 63 km, the transportation time is 60 minutes and the transportation speed is 59 km/h. The average altitude of all settlements is a level of 830 m. This altitude information means that weather conditions are of great importance in the response and will have a significant impact on weather conditions. Therefore, it will be useful to use the results obtained from this study in all disaster and emergency macro planning.

The target of reaching disasters and emergencies in 30 minutes at most in rural areas and 10 minutes in the center should be revised as shorter periods. It is possible to achieve this by establishing a "CMICEN" in the middle of a circular area with a radius of 10-20 km or a rectangular area with the same dimensions, or at a starting point that will provide convenience for transportation, taking into account the standard, quality, and transportation speed of the transportation roads.

Thus, the duration of response to disasters and emergencies can be reduced to a maximum of 20 minutes in rural areas and 5 minutes in the center. By increasing the number of centers, these durations can be shortened for the whole country (local intervention). It is thought that possibility of uninterrupted communication with CMICEN teams (with tools such as 112 Emergency Service, satellite-connected communication, and use of radio), training of officers from amateur, volunteer, or professional teams, permanent residence in that settlement, sufficient equipment to be necessary and sufficient for the results.

Acknowledgements

None declared.

Funding

The author received no financial support for the research, authorship, and/or publication of this manuscript.

Conflict of Interest

The author declared no potential conflicts of interest with respect to the research, authorship, and/or publication of this manuscript.

REFERENCES

2020 President's Annual Program, Decision No: 1733, Approval Date: November 3, 2019, Strategy and Budget Department, Ankara.

AFAD (2014). 2014-2023 Protection of Critical Infrastructure Roadmap Document. Ministry of Interior Disaster and Emergency Management Presidency, Ankara.

AFAD (2018). Turkey Earthquake Risk Map. Ministry of Interior Disaster and Emergency Management Presidency, Ankara.

Akıncı H, Doğan S, Kılıçoğlu C, Keçeci SB (2010). Production of landslide susceptibility map of Samsun province center. *Electronic Journal of Map Technologies*, 2(3), 13–27.

Altun F (2018). Economic and social impacts of disasters: An assessment of the example of Turkey. *Turkish Journal of Social Work Year*, 2(1), 1-15.

BDTİM (2017). Turkey and Tsunami Risk. Boğaçiçi University, Kandilli Observatory, and Earthquake Research Center, Regional Earthquake-Tsunami Monitoring Center, İstanbul.

Birinci F, Yılmaz MF (2020). Afet ve acil durumlar için konum, nüfus ve ulaşıma bağlı eksiklikler ve çözüm önerileri: Samsun örneği. *5. Deprem Mühendisliği ve Sismoloji Konferansı*, 8-11 October, Ankara. (in Turkish)

DBYBHY (2007). Deprem Bölgelerinde Yapılacak Binalar Hakkında Yönetmelik (Regulation for Buildings in Seismic Areas). Ministry of Public Works and Housing, Ankara. (in Turkish)

Dedeoğlu N (2017). Depremlerde Sağlık Hizmetleri. Akdeniz University, Medical School, https://www.ttb.org.tr/565ygou (Access: 23.04.2021)

Ergüney O (2007). Türkiye'nin afet profili. *TMMOB Afet Sempozyumu*, 5-7 December, Ankara. (in Turkish)

Erhan MA, Kılıç G, Çamalan G (2018). Meteorolojik Karakterli Doğal Afetler, 2017 Yılı Değerlendirmesi. T.C. Tarım Ve Orman Bakanlığı, Meteoroloji Genel MüdürlüğüAraştırma Dairesi Başkanlığı, Meteorolojik Afetler Şube Müdürlüğü, Ankara. (in Turkish)

Erkal T, Değerliyurt M (2013). The use of network analysis for emergency management in the city of Eskişehir, Turkey. *Turkish Geographical Review*, 61, 11-21.

Ersoy Ş, Nurlu M, Gökçe O, Özmen B (2017). 2016 yılında dünyada ve Türkiye'de meydana gelen doğa kaynaklı afet kayıplarının istatistiksel değerlendirmesi. *Mavi Gezegen Popüler Yerbilim Dergisi*, 22, 13-27. (in Turkish)

Gökçe O, Özden Ş, Demir A (2008). Türkiye'de Afetlerin Mekansal ve İstatistiksel Değılımı Afet Bilgileri Envanteri. Bayındırlık ve İskan Bakanlığı Afet İşleri Genel Müdürlüğü, Ankara. (in Turkish)

İçişleri Bakanlığı (2004). Türkiye'de Doğal Afetler Konulu Ülke Strateji Raporu. Japonya Uluslararası İşbirliği Ajansı (JICA) Yayınları, Türkiye Ofisi, Ankara. (in Turkish)

Keleş R (2002). Kentleşme Politikası. İmge Kitapevi, Ankara. (in Turkish)

Özmen, B (2012). The historical development of seismic zoning maps of Turkey. *Geological Bulletin of Turkey*, 55(1), 43-55.

Özşahin E (2013). Türkiye'de yaşanmış (1970-2012) doğal afetler üzerine bir değerlendirme. *2. Deprem Mühendisliği ve Sismoloji Konferansı*, 25-27 September, Hatay, Turkey. (in Turkish)

Republic of Turkey Ministry of Natural Defense General Directorate of Mapping (2021). Provincial and District Areas, https://www.harita.gov.tr/urun/il-ve-ilce-yuzolcumleri/176 (Access: 15.02.2021).

Şahin K (2013). The responsibility of the state in case of a natural disaster under the law of ECHR in the context of right to life and right to property: Budayeva judgment. *Marmara Üniversitesi Hukuk Fakültesi Hukuk Araştırmaları Dergisi*, 19(3), 53-146.

TBDY (2018). Turkish Seismic Design Code. Ministry of Interior Disaster and Emergency Management Presidency, Ankara.

TÜİK (2021). Address Based Population Registration System (ADNKS), https://biruni.tuik.gov.tr/medas/?kn=95&locale=tr (Access: 12.02.2021)

Tüney S (2015). From the legal perspective of emergency management and temporary protection status and Turkey's legislation and practices in Syrian crisis. Institute of 71 Research, Learning and Development, Retrieved on April 24, 2022.

Challenge Journal of Structural Mechanics

Research Article

Investigation of mechanical properties of steel reinforcements in reinforced concrete structures as a result of exposure to fire

Abdulhadi Koşatepe [a,*], Casim Yazici [b]

[a] *Patnos Vocational School, Ağrı İbrahim Çeçen University, 04500 Patnos, Ağrı, Türkiye*
[b] *Doğubayazıt Ahmed-i Hani Vocational School, 04400 Doğubayazıt, Ağrı, Türkiye*

ABSTRACT

In this study, it is aimed to investigate the properties of the most commonly used metal and alloy steel materials, which are used in our country and in the world as engineering materials, under the influence of fire of the rebar in the concrete. Inspection standard TS 708:2010 S420 quality 8 mm diameter ribbed construction iron bars for 90 minutes in resistant furnace, atmospheric environment at 600 °C, 800 °C and 1000 °C concrete inside and outside the concrete at the specified temperature fire simulation, the process was allowed to cool in air. With the protective environment created by reinforced concrete, the temperature directly affecting steel bars located outside the concrete under the same conditions, The variable properties of the sample, which are inside the concrete and outside the concrete, were evaluated comparatively. Surface images of the specimens prepared in metallography were taken at different magnifications. The tensile strength of rebar bars did not change significantly according to the environment, but the samples in the concrete showed a more ductile tendency than the samples outside the concrete. The hardness values of the steel bars in the concrete and the steel bars other than the concrete decreased as the temperature increased and this decrease was higher in the samples in the concrete.

ARTICLE INFO

Article history:
Received 2 January 2023
Revised 11 February 2023
Accepted 18 March 2023

Keywords:
Fire effect
Hardness
Steel
Tensile strength

1. Introduction

It is known that iron and its alloys take the first place among the materials used in the field of engineering. Iron alloy steels constitute a large part of these materials.

The physical, chemical and mechanical properties of steels to be used are decided according to the working conditions. While commonly formed structures are selected according to these characteristics, exposure to high temperatures is generally ignored (Uysal 2004; Buzkıran et al. 2016). Mechanical properties of steel at high temperature, such as yield limit, ultimate strength, hardness, modulus of elasticity and thermal expansion coefficient, are the basic mechanical properties that determine the high temperature performance of steels (Ketabdari et al. 2019; Demirel and Özkan 2003). Fire is a serious threat to all building elements and causes loss of life and property. In this context, although steel structures or steel-containing structures show superior properties at room temperature, they are materials that show a significant decrease in their strength at high temperatures due to their metallurgical structures. (Köksal et al. 2004; Kodur and Aziz 2015; Cirpici et al. 2022). While steel structural elements have high strength and rigidity under normal conditions, these properties deteriorate rapidly at relatively high temperatures of 600 °C and above, and fire seriously reduces the load bearing capacity of the structure Yazici et al. (2022). Steel structures should not only have the capacity to carry the design loads at room temperature, but also maintain their strength in the face of difficult events such as fire in structural design. For this reason, fire resistant designs of these structures should be made so that the structures can maintain sufficient strength at high temperatures within the fire resistance period (Ergün et al. 2010). A large part of the building stock consists of re-

* *Corresponding author*. Tel.: +90-472-502-3050 ; Fax: +00-000-000-0000 ; E-mail address: akosatepe@agri.edu.tr (A. Koşatepe)
ISSN: 2149-8024 / DOI: https://doi.org/10.20528/cjsmec.2023.02.003

inforced concrete and steel carrier systems added as carriers into the reinforced concrete structure. Because it is a semi-insulating material due to its structure and is more resistant to fire than steel, the concrete covering the steel creates thermal insulation for the steel (Buzkıran and Erten 2016).

Scientific studies are continuing on environmental coating with concrete and thermal swelling coating applications in order to use it as a thermal barrier against fire on structural elements and materials (Zhao et al. 1999; Ergün et al. 2010; Atashafrazeh et al. 2022). Steel and concrete are in the group of non-combustible materials in terms of flammability. Since they are non-combustible, there is no material loss in fire damage, but great decreases are observed in hardness values, yield limit and tensile strength in all post-fire steels (Tama 2012; Kodur et al. 2015). However, with the diffusion of nitrogen atoms in the microstructure at around 200 °C to the grain boundaries, a slight increase in the tensile strength and hardness of the steels is observed. However, when 300 °C is exceeded, the hardness and strength values begin to decrease. When the temperature rises above the critical threshold of 600 °C, the tensile strength falls below the safe mechanical values (Tama 2012; İplikçi 2006; Aliş et al. 2022).

In this study, the grain structures, tensile strength and hardness values of ribbed construction steels inside and outside the concrete were comparatively examined under the easily accessible temperatures of 600 °C, 800 °C and 1000 °C during fire. In addition, surface images were taken with a scanning electron microscope and their chemical compositions were examined.

2. Material and Method

Steel, which is the most widely used engineering material among metals, has some superior properties that make it advantageous compared to other building materials and highlight its use. Some of these are properties such as high strength and high modulus of elasticity of steels (Tama and Kaftan 2007).

Basically, fire consists of 5 phases: ignition, development, growth, full growth and extinction (İplikçi 2006; Korol et al. 2015). In a combustion event, the temperature relationship according to the fire stages is given in Fig. 1 (Yazıcı and Koşatepe 2020).

The variation in the temperature of protected and unprotected structural steels during fire is given in Fig. 2 depending on the time.

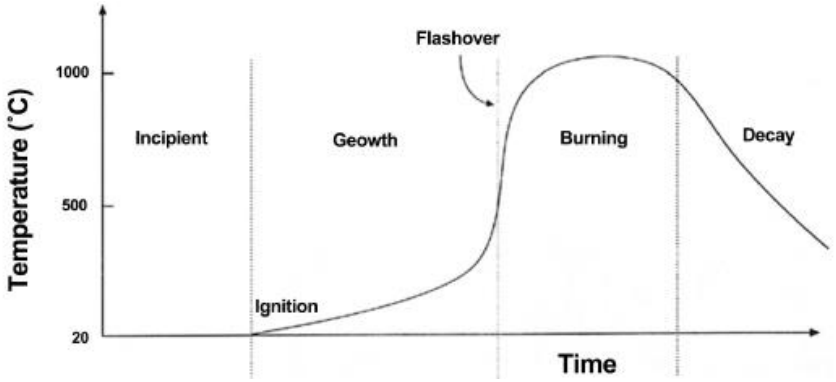

Fig. 1. Classic fire development curve (Polzin 2019).

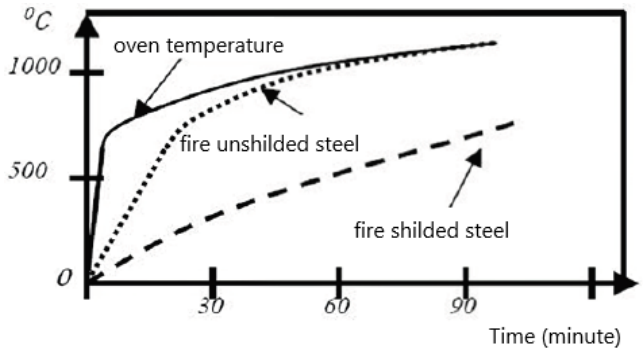

Fig. 2. Time-temperature relationship in structural steels (Lawson 2001).

In this study, TS 708:2010 standards and 8 mm diameter ribbed construction steel were placed in the concrete by leaving a 3 cm spacer. Then, the samples were kept at 600 °C and 1000 °C temperatures for 90 minutes and then allowed to cool. The temperature regulated furnace used to create an environment similar to the fire environment is given in Fig. 3. The samples were left to cool in the air after the fire as shown in Fig. 4.

Considering the fire conditions, 15 cm long and 8 mm diameter ribbed construction steel was embedded in the cement mixture (called C30) used in the structures. Then, 7 days were waited for the cement to cure. Concrete blocks containing steel in the form of molds were kept in the furnace for 90 minutes, being exposed to temperatures of 600 °C, 800 °C and 1000 °C separately. It was then removed from the furnace and left to cool in air for 24 hours. In this study, the samples inside the concrete will be called as “Intra-Concrete” (I.C.), and the samples outside the concrete will be called as “Non-Concrete” (N.C.).

I.C. and N.C. samples exposed to temperatures were classified for metallographic preparation. In order to obtain the surface images and measure the hardness values, it was cut into certain sizes and placed in the bakelite container. Then, it was sanded according to the appropriate abrasive sizes (240-2000 mesh) and polishing (crystal liquid containing 1 μm particles) processes were performed.

Fig. 3. Ash furnace providing desired temperatures.

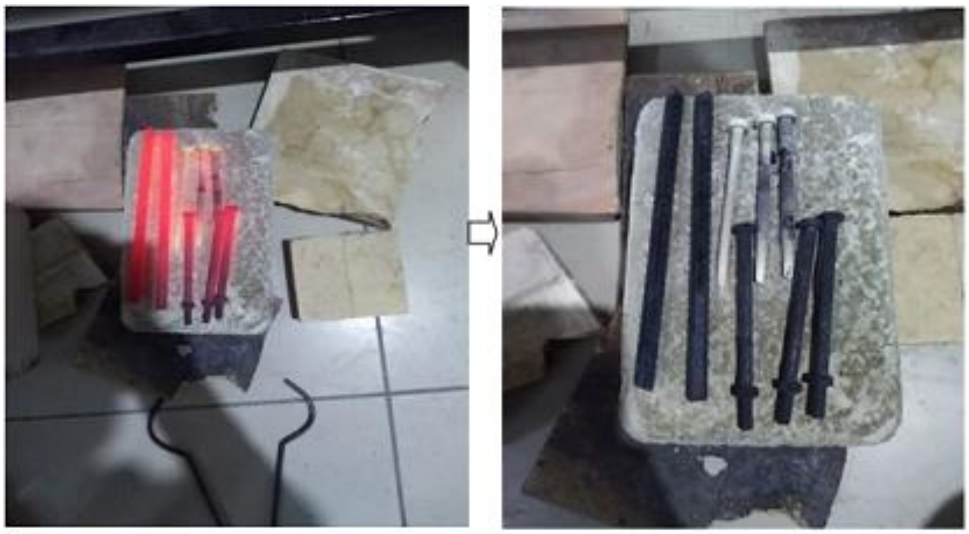

Fig. 4. Samples inside and outside the concrete that were left to cool in air.

Using a Nikon Eclipse LV150 metal microscope, surface images of samples subjected to sanding and polishing were obtained at magnifications of 50X, 100X and 200X. Then, the hardness values of the samples were measured under a load of 200 g using the Wolpert Wilson Instruments Vickers hardness tester. Using the SHIMADZU brand tensile device, the tensile strengths of the samples prepared according to ASTM E8:2016 standards were determined at a loading speed of 5 mm/min. Finally, using the Zeiss Sigma 300 SEM device, the surface topography of the samples was taken and the surface composition was examined with the EDAX software. The obtained results were examined comparatively in the form of in-concrete and out-concrete samples.

3. Experimental Results

Using a metal microscope, the surface images of the cross-sections of the concrete and non-concrete samples tested were obtained at the mentioned magnification ratios and are given in Figure 5 and Figure 6. Depending on the effect of temperature and cooling rate, it is clearly seen that an integrated structure is formed on the surfaces of both non-concrete (N.C.) and intra-concrete (I.C.) samples at various magnifications.

Considering the images taken from the sample at room temperature given in Fig. 5, it is seen that the porous structure seen on the surface decreases as the temperature increases at all magnification ratios in non-

conc-rete samples. However, as seen in Fig. 6, the hollow structure seen on the surface of the steel sample at room temperature in the concrete samples decreases up to 800 °C, but after 800 °C is exceeded, it is observed that the hollow structure is more than the sample at room temperature.

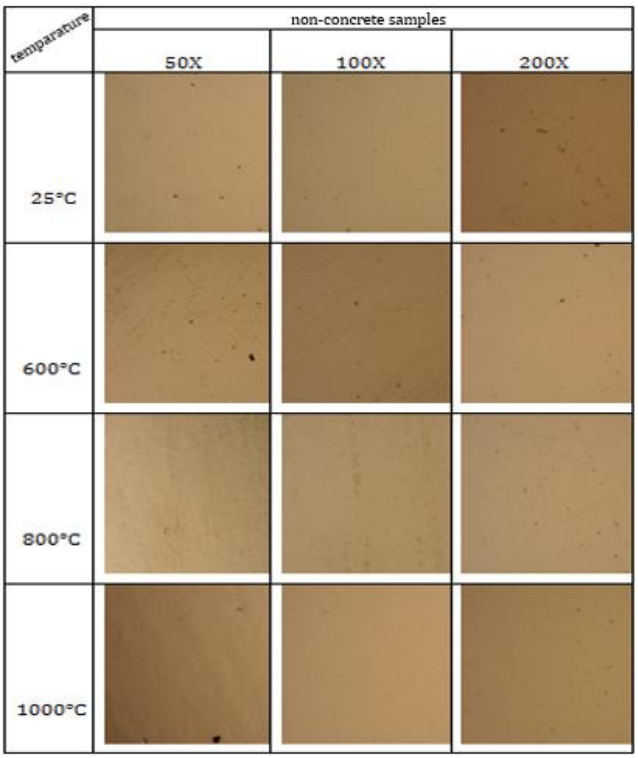

Fig. 5. Surface images of non-concrete samples taken under the metal microscope at the specified magnifications.

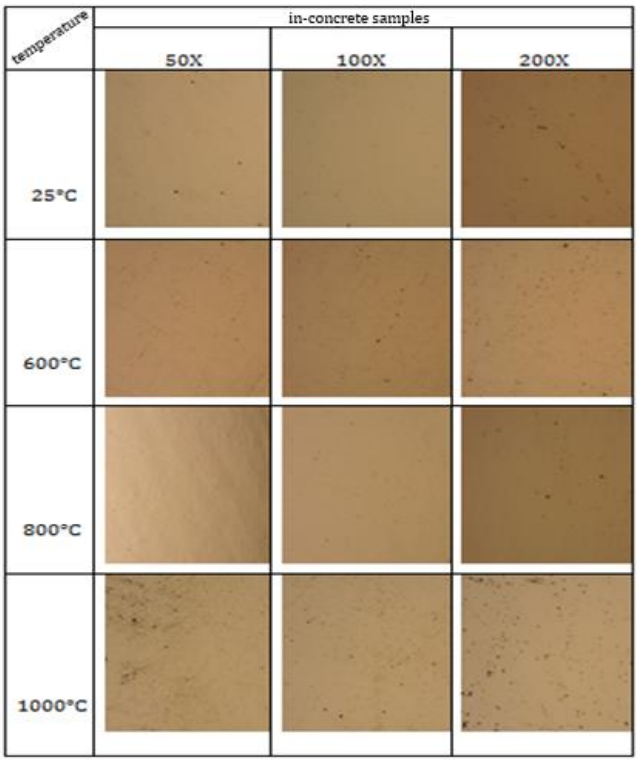

Fig. 6. Surface images of the samples in the concrete taken at the specified magnifications under the metal microscope.

Using a metal microscope, surface images of the samples inside and outside the concrete in case of fire were obtained. In addition, SEM images obtained at 100 μm size are given in Figs. 7 and 8. In the structures of the samples outside the concrete, it is seen that the number of voids seen on the surface decreases as the temperature increases and turns into a more integrated structure. In the samples in the concrete, it was observed that the voids decreased up to 800 °C, but it was determined that the voids increased again after 800 °C.

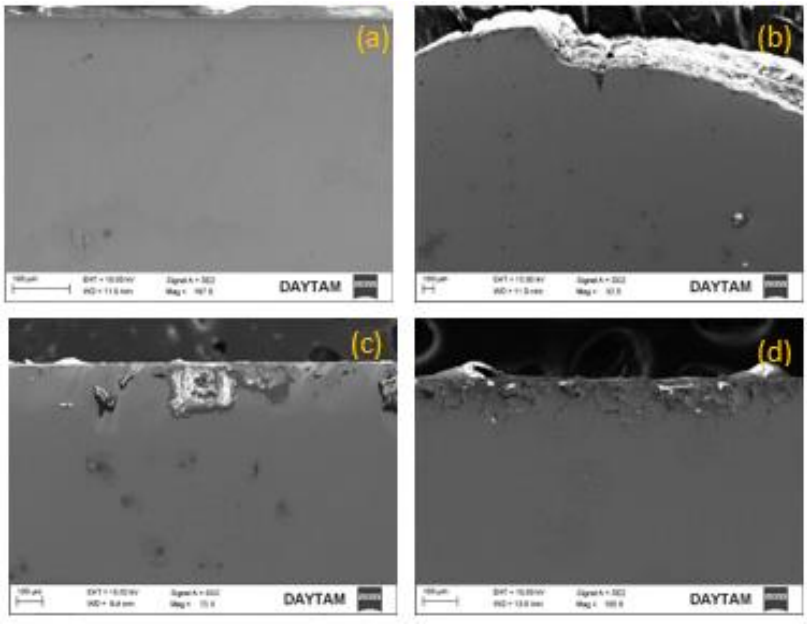

Fig. 7. SEM images of non-concrete samples: (a) at 25 °C; (b) at 600 °C; (c) at 800 °C; (d) at 1000 °C.

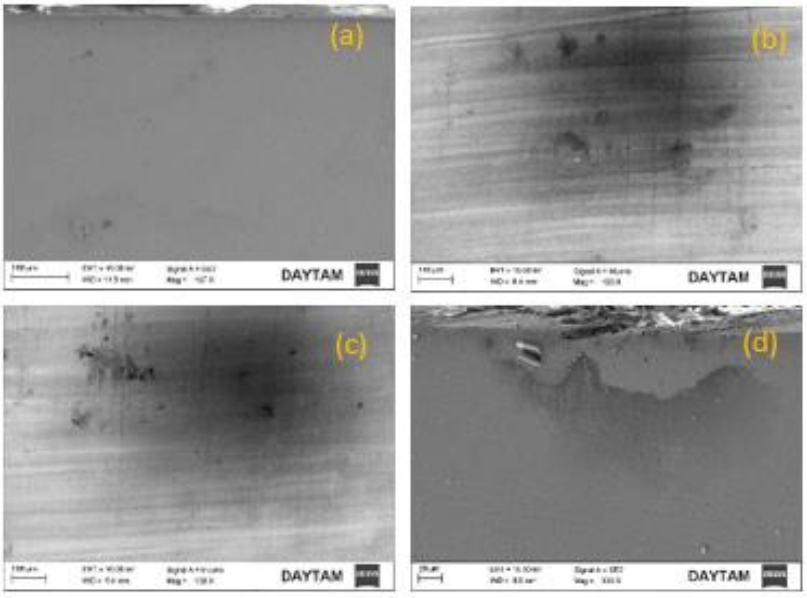

Fig. 8. SEM images of samples in concrete: (a) at 25 °C; (b) at 600 °C; (c) at 800 °C; (d) at 1000 °C.

Contrary to the heat treatments applied to steels, it is known that as a result of uncontrolled heating and cooling, the steel, both inside and outside the structure, loses most of its strength due to the high temperature.

As can be seen in Fig. 9, the hardness of steels decreases as the temperature increases and the cooling rate decreases. It has been determined that the decrease in the hardness values of the steels outside the concrete is higher than the decrease in the hardness values of the steels inside the concrete.

In Figs. 10 and 11, the samples subjected to the tensile test are handled separately as in-concrete and non-concrete. It is observed that the tensile strengths of both in-concrete and non-concrete samples do not change significantly up to 600 °C. However, at 800 °C and 1000 °C, a very significant decrease in tensile strength is observed for both in-concrete and non-concrete samples. Similarly, while there is no significant change in the ductility of the samples up to 600 °C, it is seen that the ductility values increase as the temperature increases. In the strength values parallel to the hardness properties, both the tensile strength of the in-concrete samples and the tensile strength of the non-concrete samples decreased. It was determined that the strength of the in-concrete samples decreased more than the strength of the non-concrete samples. Contrary to the hardness and strength values, the ductility values increased as the temperature increased.

As seen in Fig. 12, the steel sample outside the concrete melted locally at 600 °C. As given in Table 1, it has been determined that the oxygen rate seen on the surface is quite high. However, as can be seen in Fig. 13, it is seen that instead of regional melting, cavities are formed in the sample in the concrete. In addition, as seen in Table 2, it was determined that the oxygen ratio was low. Significant differences were observed on the surfaces of the in-concrete and non-concrete samples in terms of compositions.

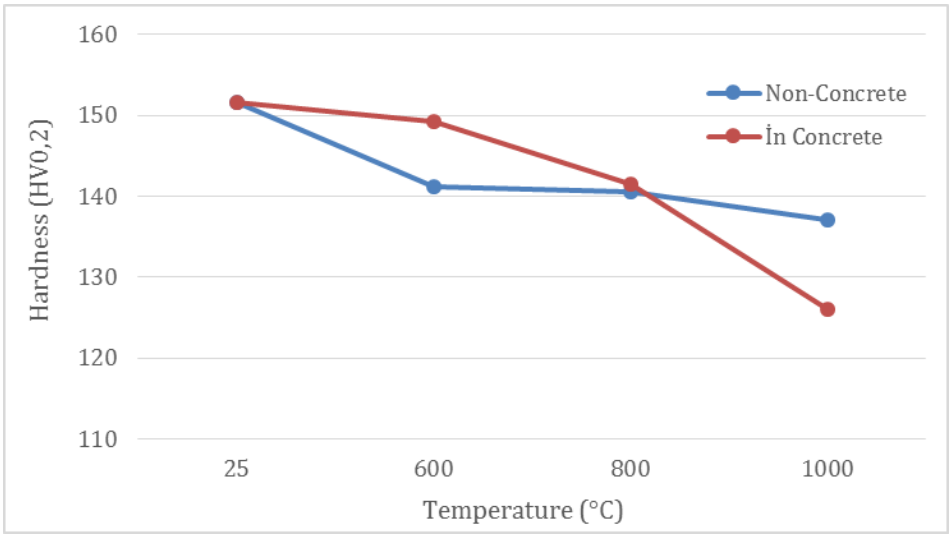

Fig. 9. Hardness values of samples inside and outside concrete.

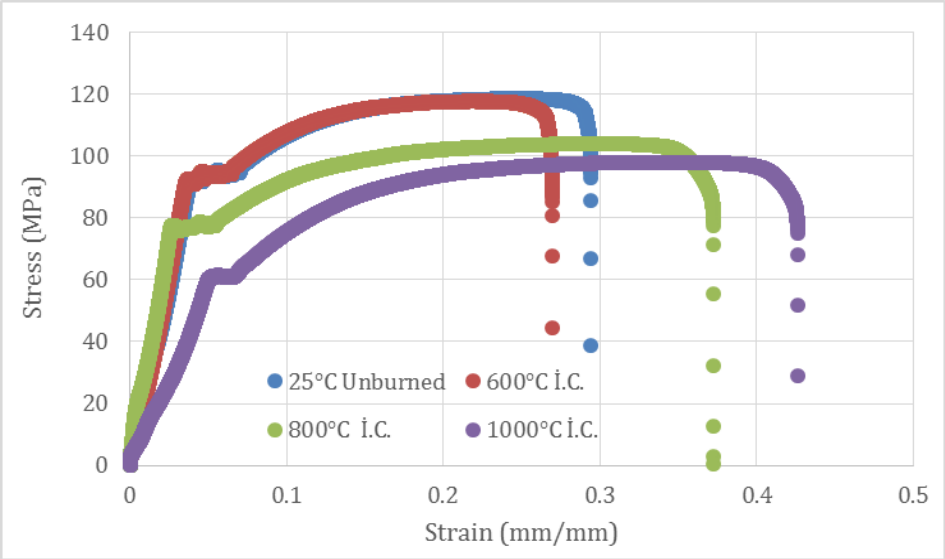

Fig. 10. Tensile curves of samples in concrete.

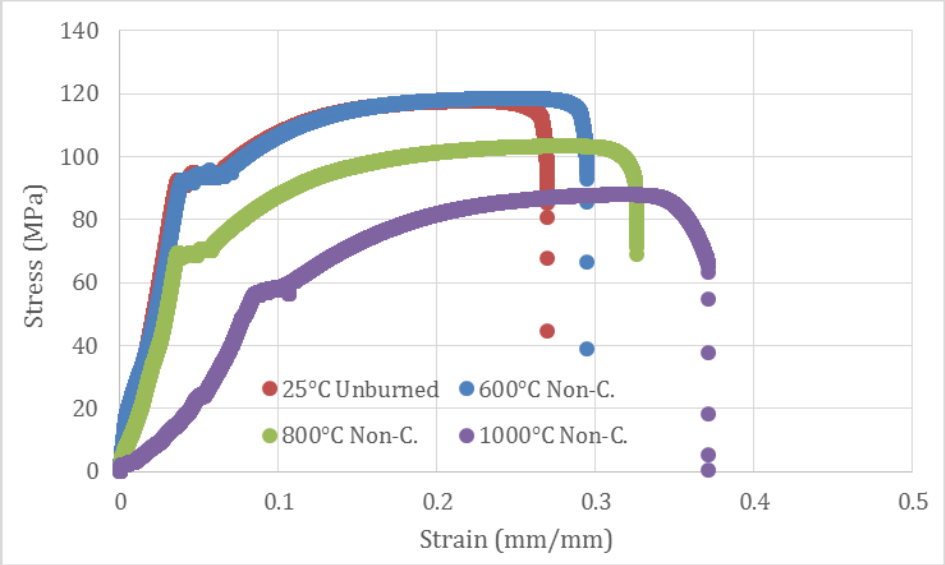

Fig. 11. Tensile curves of non-concrete samples.

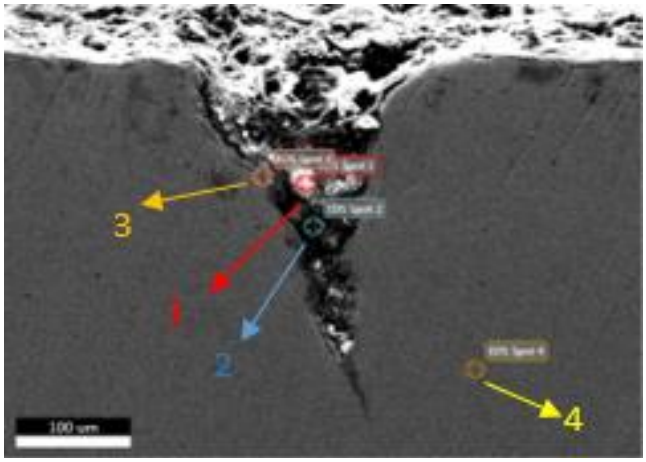

Fig. 12. SEM image of non-concrete steel at 600 °C.

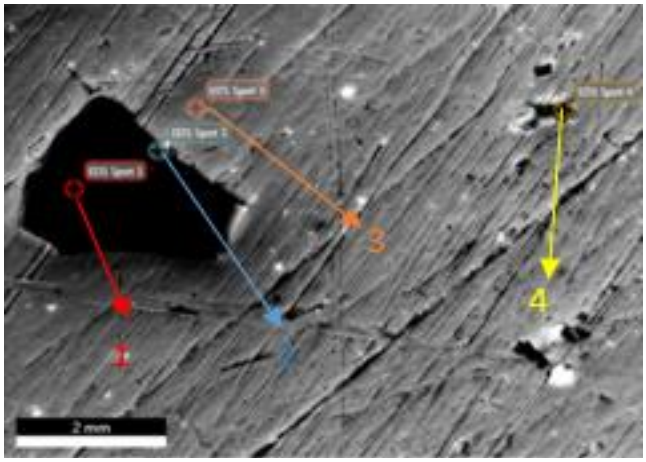

Fig. 13. SEM image of steel in concrete at 600 °C.

Table 1. Compositions of the regions in the SEM image of the sample treated on-concrete at 600 °C.

EDS Spot1		
Element	Weight %	Atomic %
C K	8.0	13.4
O K	48.4	61.1
NaK	2.5	2.2
MgK	0.6	0.5
AlK	1.9	1.4
SiK	9.4	6.8
FeK	1.9	0.7

EDS Spot2		
Element	Weight %	Atomic %
C K	46.8	63.0
O K	22.2	22.4
FeL	0.2	0.0
NaK	3.0	2.1
MgK	0.3	0.2
AlK	1.3	0.8
SiK	4.9	2.8

EDS Spot3		
Element	Weight %	Atomic %
O K	26.4	55.5
SiK	0.2	0.3
CaK	0.2	0.2
FeK	73.2	44.1

EDS Spot4		
Element	Weight %	Atomic %
C K	0.5	2.2
O K	2.5	8.2
SiK	0.2	0.3
FeK	96.8	89.3

Table 2. Compositions of the regions in the SEM image of the sample treated in concrete at 600 °C.

EDS Spot1		
Element	Weight %	Atomic %
C K	10.5	29.7
O K	6.0	12.9
AlK	0.2	0.3
SiK	10.3	12.5
FeK	73.0	44.6

EDS Spot2		
Element	Weight %	Atomic %
C K	32.8	63.8
O K	5.0	7.2
AlK	0.0	0.0
SiK	7.1	5.9
FeK	55.1	23.0

EDS Spot3		
Element	Weight %	Atomic %
O K	1.6	5.3
SiK	0.2	0.3
FeK	98.2	94.3

EDS Spot4		
Element	Weight %	Atomic %
C K	10.0	31.8
O K	3.7	8.8
CaK	0.9	0.9
FeK	85.4	58.4

In Fig. 14, it was seen that local melting and agglomeration were observed in the steel samples treated at 1000 °C other than concrete. In the composition samples taken from these regions, it was determined that the carbon atoms were gathered together as given in Table 3. It has been observed that both carbon and oxygen ratios decrease significantly towards the inside of the steel, where the oxygen ratio is high on the surface.

In Fig. 15, local melting and agglomeration were not observed in the sample placed in the concrete at 1000 °C. In Table 4, the element ratios in the inner sections of the steel are given. In this table, it is seen that the oxygen rate is very low.

The cavities formed in the steel exposed to the heat in the concrete are given in Fig. 16. Micro cracks and structural defects occurred in the cavity.

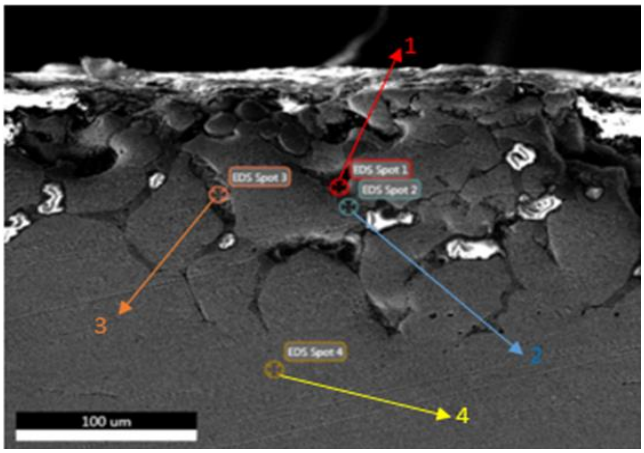

Fig. 14. SEM image of steel non-concrete at 1000 °C.

Table 3. Compositions of the regions in the SEM image of the sample treated non-concrete at 1000 °C.

EDS Spot1		
Element	Weight %	Atomic %
C K	10.6	26.2
O K	17.4	32.4
AlK	2.2	2.5
SiK	1.2	1.2
S K	0.7	0.6
CaK	3.6	2.7
MnK	7.4	4.0
FeK	56.8	30.3

EDS Spot2		
Element	Weight %	Atomic %
O K	29.9	59.7
CaK	0.3	0.2
MnK	0.6	0.3
FeK	69.3	39.7

EDS Spot3		
Element	Weight %	Atomic %
O K	17.9	41.3
MnL	0.7	0.5
SiK	0.1	0.1
S K	9.4	10.7
FeK	71.9	47.4

EDS Spot4		
Element	Weight %	Atomic %
C K	0.7	2.9
F K	4.2	11.1
SiK	0.3	0.6
MnK	0.5	0.5
FeK	94.3	84.9

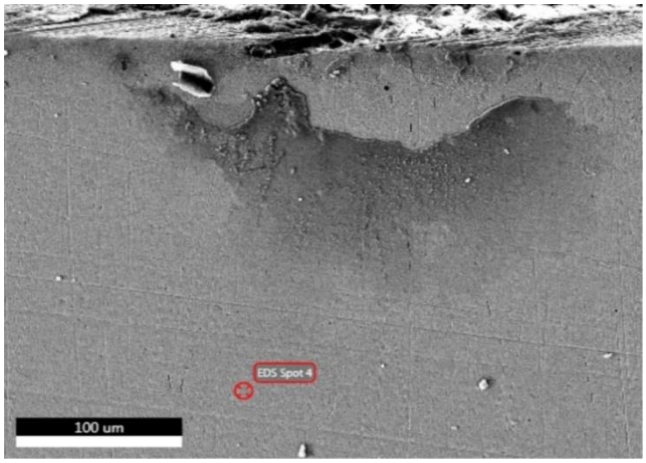

Fig. 15. SEM image of the sample treated in concrete at 1000 °C.

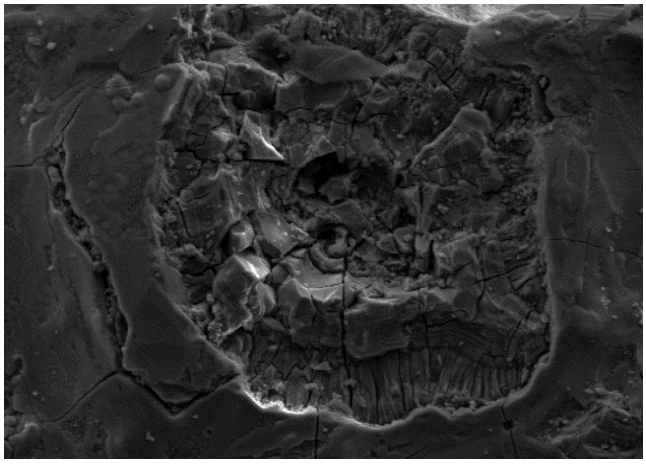

Fig. 16. SEM image of the cavity formed on the surface of the steel treated in concrete at 1000 °C.

Table 4. Composition of the region in the SEM image of the sample treated in concrete at 1000 °C.

EDS Spot4		
Element	Weight %	Atomic %
C K	0.0	0.1
F K	1.2	3.9
MnK	0.3	0.3
FeK	98.5	95.7

4. Conclusions

The following results were obtained in this research, in which the situations of the presence of ribbed construction steel exposed to fire in concrete (I.C.) and outside of concrete (N.C.) were studied comparatively. Microstructural, physical and chemical properties of the ribbed construction steels inside and outside the concrete are determined by the effect of temperature in the event of fire.

The steel embedded in the concrete heats up together with the concrete during the fire. The samples inside the concrete heat up and cool down more slowly than the samples outside the concrete. In this case, it was determined that the number of voids in the samples inside the concrete was higher than the samples outside the concrete. Similar to the studies in the literature, in this study, it is seen that the grains of the steels inside the concrete are larger than the grains of the steels outside the concrete, depending on the effect of temperature and the cooling rate. The high number of coarse grains reduces the number of grain boundaries in the structure. With the decrease in the number of grain boundaries in the material, the strength and hardness values of the material decrease. However, due to the slow cooling rate, it is

seen that this decrease is more in the steels in the concrete. Grain growth, which caused a decrease in hardness and strength, also caused an increase in ductility, as expected.

In line with the information obtained from previous studies, it can be deduced that the reason for the high rate of oxygen in the composition samples taken from the areas close to the surface of the steels is that the temperature increase in the material accelerated the oxidation. In the steels in the concrete, the bond of the steel with the oxygen is relatively cut due to the protective atmosphere created by the concrete. Therefore, it is determined that the amount of oxygen on the surface of the steels in the concrete is quite low. In addition to the heat treatments applied to the steels, the pits formed on the surface of the steel material and in the steel material after uncontrolled heating and cooling reduce the strength and hardness of the material. It is very clear that the concrete and steel to be used in construction works should be designed by taking into account disasters such as fire. If the continuity of the structure is to be ensured after disasters, it is extremely important to evaluate it by taking these results into account.

Acknowledgements

The authors would like to present their thanks to Department of Metallurgical and Materials Engineering, Engineering Faculty, Atatürk University for their support.

Funding

The authors received no financial support for the research, authorship, and/or publication of this manuscript.

Conflict of Interest

The authors declared no potential conflicts of interest with respect to the research, authorship, and/or publication of this manuscript.

References

Aliş B, Yazici C, Özkal FM (2022). Investigation of fire effects on reinforced concrete members via finite element analysis. *ACS Omega*, 7(30), 26881-26893

Atashafrazeh M, Bingöl AF, Caf M (2017). The influence of elevated temperatures on the mechanical properties of polypropylene fiber reinforced concrete. *Challenge Journal of Structural Mechanics*, 3(3), 116-122.

Buzkıran C, Erten E (2016). A research on fire behavior of high-rise steel and reinforced concrete structures. *Çukurova University Journal of Science and Engineering*, 34(2).

Cirpici BK, Orhan SN, Yazici C, Özkal FM (2022). Numerical investigation of the fire behavior of storage rack systems protected by intumescent coating. *ACS Omega*, 7(40), 36001-36008.

Demirel F, Özkan E (2003). Steel structure components and fire safety precautions. *Gazi University Faculty of Engineering and Architecture Journal*, 18(4), 89-107.

Ergün A, Kürklü G, Başpınar MS (2010). Investigation of mechanical properties of reinforced concrete steels of different classes after high temperature. *Afyon Kocatepe University Journal of Science*, 9(2), 97-103.

İplikçi E (2006). Analysis of Fire Safety Measures in Buildings and Determination of Performance Criteria for Fire Safe Building Design. *M.Sc. thesis*, Gazi University, Ankara.

Ketabdari H, Daryan AS, Hassani N (2019). Predicting post-fire mechanical properties of grade 8.8 and 10.9 steel bolts. *Journal of Constructional Steel Research*, 162, 105735.

Kodur VK, Aziz EM (2015). Effect of temperature on creep in ASTM A572 high-strength low-alloy steels. *Materials and Structures,* 48, 1669-1677.

Kodur VK, Naser MZ, Aziz E (2015). Strategies for enhancing fire performance of steel bridges. *Fifth International Workshop on Performance, Protection & Strengthening of Structures under Extreme Loading*, East Lansing, MI, USA, June 28–30.

Köksal NS, Uzkut M, Ünlü BS (2004). Change of mechanical properties of steels with different carbon contents by heat treatments. *Dokuz Eylül University Faculty of Engineering Journal of Science and Engineering*, 6(2), 95-100.

Korol R, Greening F, Heerema P (2015). Performance-based fire protection of office builds: A case study based on the collapse of WTC7. *Challenge Journal of Structural Mechanics*, 1(3), 96-105.

Lawson RM (2001), Fire engineering design of steel and composite buildings. *Journal of Constructional Steel Research*, 57, 1233–1247.

Polzin SS, Saupe A, Krause U (2019). Horizontal fire spread in a contemporary apartment based on a real fire. *Open Journal of Civil Engineering*, 9, 367-385.

Tama YS (2012). Fire protection of steel structures. *Steel Structures*, Technical Article, Issue 32.

Tama YS, Kaftan A (2007). Investigation of corrosion protection cost in steel structures. *2nd National Symposium on Steel Structures*, TMMOB Chamber of Civil Engineers, Eskişehir.

Uysal A (2004). Effects of High Temperature on Concrete. *M.Sc. thesis*, İstanbul Technical University, İstanbul, Türkiye.

Yazıcı C, Koşatepe A (2020). Experimental investigation of fire effect of composition elements in steel structures. *Iğdır Journal of the Institute of Science and Technology of the University*, 10(4), 2692-2703.

Yazici C, Özkal FM, Orhan SN, Cirpici BK (2022). Reformative effects of intumescent coating on the structural characteristics of cold-formed steel. *ACS Omega*, 7(46), 42560–42569.

Zhao JC, Shen ZY (1999). Experimental studies of the behaviour of unprotected steel frames in fire. *Journal of Constructional Steel Research*, 50, 137- 150.

Challenge Journal of Structural Mechanics

Research Article

Effects of pre-cracked reinforced concrete in compression zone on prefabricated RC beam behavior

Mahmut Cem Yılmaz [a,*]

[a] *Department of Civil Engineering, Ankara Yıldırım Beyazıt University, 06010 Ankara, Türkiye*

ABSTRACT

Cracks can occur in the compression zone of a beam cross section, in the middle part of the span due to different reasons. For instance, due to accidents happened during transportation of the prefabricated Reinforced Concrete (RC) beams on manufacturing site. In this study, effects of such cracks on the behavior of RC beams are investigated experimentally. Compression strength of concrete and intensity degree of pre-created cracks were adopted as test parameters. A total of eight RC beam specimens were tested under the effect of bending, applying three-point loading. According to the results it was observed that the pre-cracked RC beams had almost the same strength with the reference beams; but bending stiffness of the RC beams decreased when the intensity of the cracks increased relatively.

ARTICLE INFO

Article history:
Received 23 December 2022
Revised 23 January 2023
Accepted 18 March 2023

Keywords:
Prefabricated RC beam
Cracks intensity
Bending
Stiffness

1. Introduction

Due to accidents happened during transportation of the prefabricated Reinforced Concrete (RC) beams on manufacturing site, cracks can occur in the compression zone of a RC beam cross section, in the middle part of the span (Fig. 1). In the current structures, similar cracks can also occur in the RC beams because of earthquake effects. Compression zone has a significant impact on beam bearing capacity. Thus, it is thought to be an important question to investigate how these types of cracks affect the beam behavior. Since this topic in literature was not tackled directly, as to our knowledge, it is decided to conduct this research.

In this study, the effects of pre-created cracks, in compression zone of the section in the middle part of the span, on the behavior of RC beams were investigated experimentally. The parameters of the experiment were essentially the intensity degree of the pre-created cracks and the compression strength of concrete. To conduct the experiment in the lab, a total of eight RC beams were prepared with a 1/3 scale of applicable dimensions in real structures. The Specimens were tested under the effect of bending applying three-point loading.

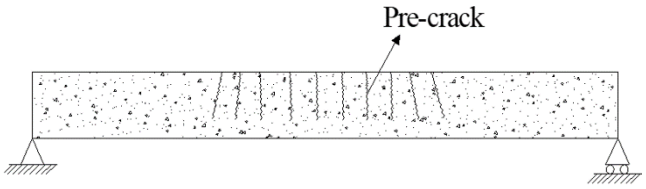

Fig. 1. Pre-cracked reinforced concrete beam.

In previous studies, usually the cracks were pre-created in the tension zone of the beam section in the span middle part, or in the shear segment of the beam close to the supports. In these research, it is noticed that Arnaud Castel, a researcher in University of New South Wales (Australia), stands out with significant experimental and theoretical studies. In his studies, deflection of the pre-cracked beams and their static (Castel et al. 2012, 2013, 2014; Castel and François 2013; Xu et al. 2018a, 2018b) and dynamic (Xu and Castel 2016; Xu et al. 2018c) stiffness were examined, and the accuracy of the proposed models and methods were investigated. Along with these studies, there are some other theoretical and experimental studies conducted by other researchers about

* *Corresponding author*. Tel.: +90-312-906-2298 ; E-mail address: mcemyilmaz@ybu.edu.tr (M. C. Yılmaz)
ISSN: 2149-8024 / DOI: https://doi.org/10.20528/cjsmec.2023.02.004

efective shear stiffness (Pan et al. 2014), long-term deflections (Rahman et al. 1998), various creep analysis (Zhang and Hamed 2020) and long-term flexural behavior (Sryh and Forth 2022) of pre-cracked beams. Reviewing the literature, it is concluded that the pre-cracked beams in compression zones were not investigated thoroughly despite the importance of compression zone for the beams' strength and behavior.

2. Experimental Study

2.1. Test specimens and materials

A total of eight 1/3 scale RC beams were tested under the effect of bending, applying three-point loading. Each specimen had a length of 1000 mm and rectangular cross section of 100 mm width and 150 mm height. All beams had the same reinforcement configuration shown in Fig. 2. Specimens were reinforced with two longitudinal ribbed bars of 8 mm diameter at the top, three longitudinal ribbed bars of 8 mm diameter at the bottom of the cross section. The longitudinal ribbed bars were of grade S420. Beams were also reinforced with stirrups of 4 mm diameter spaced at 60 mm. Stirrups were of plain bars.

100x100x100 mm size cubic concrete specimens were tested to obtain the compressive strength of the concrete. One group of 4 beams had a concrete compressive strength of 45 MPa (36 MPa for standard cylindrical sample) and the other group had a concrete compressive strength of 55 MPa (44 MPa for standard cylindrical sample).

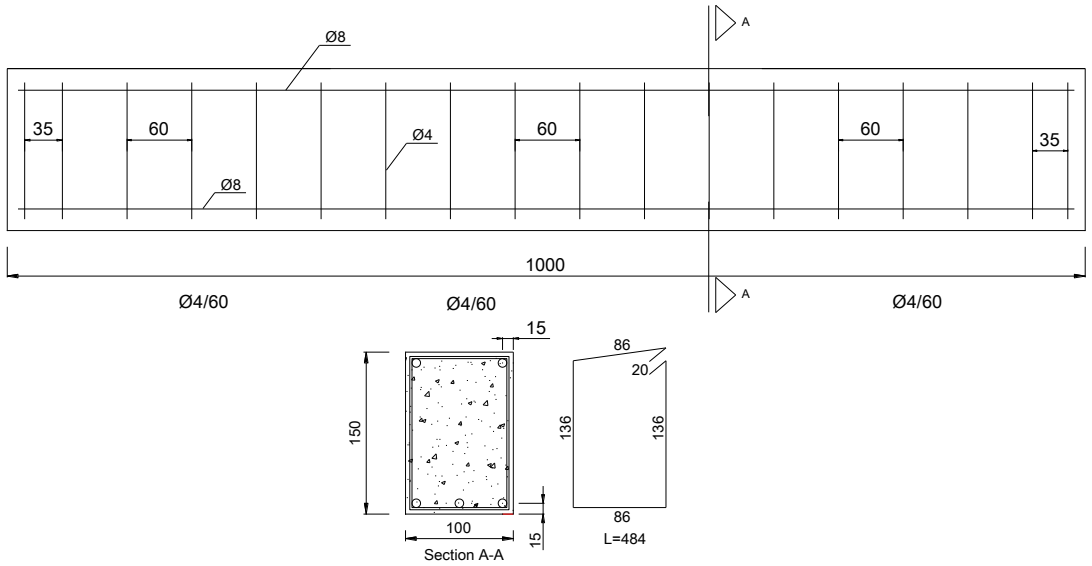

Fig. 2. Reinforcement dimension and configuration of the tested RC beams.

Before the testing, cracks with different intensity were created, in the compression zones of the sections in the middle part of the span, by loading the beams placed upside-down on the bending test setup. No cracks were created on the reference beams. Degree of the pre-created cracks' intensity of the least damaged specimen was identified by number 1 and of the most damaged specimen was identified by number 6. As the identification number increases the crack intensity and damage level increases. For the non-pre-cracked beams (reference beams) the number 0 is used. The number of cracks, crack width and depth were considered to determine the pre-created cracks' intensity degree.

Test specimens were named as RB45-0, B45-1, B45-2, B45-3, RB55-0, B55-4, B55-5 and B55-6. The specimens RB45-0 and RB55-0 were reference beams. The first two digit refers to the compressive strength of the concrete. Final digit refers to the degree of the intensity of the pre-created cracks. For example: the specimen named as B45-2 has a concrete compressive strength of 45 MPa and degree of pre-created crack intensity 2. Pre-created crack damages of each RC beam were shown in Fig. 3. Table 1 shows the compressive strength and degree of pre-created crack intensity of each specimen.

Table 1. Properties of the tested RC beams.

Name of the specimen	Compressive strength of concrete (MPa)	Degree of intensity of pre-crack
RB45-0	45	0
B45-1	45	1
B45-2	45	2
B45-3	45	3
RB55-0	55	0
B55-4	55	4
B55-5	55	5
B55-6	55	6

2.2. Test setup and instrumentations

RC beams were tested by the bending test setup, applying three-point loading (Fig. 4). RC beam specimens were placed on the test setup with simple support. A concentrated load was applied on the span midpoint of the beams by a load cell having a capacity of 20 kN. An elec-

tronic displacement measure device was used to measure the deflection at the span midpoint. Obtained load and deflection data were transferred to the computer by a data logger.

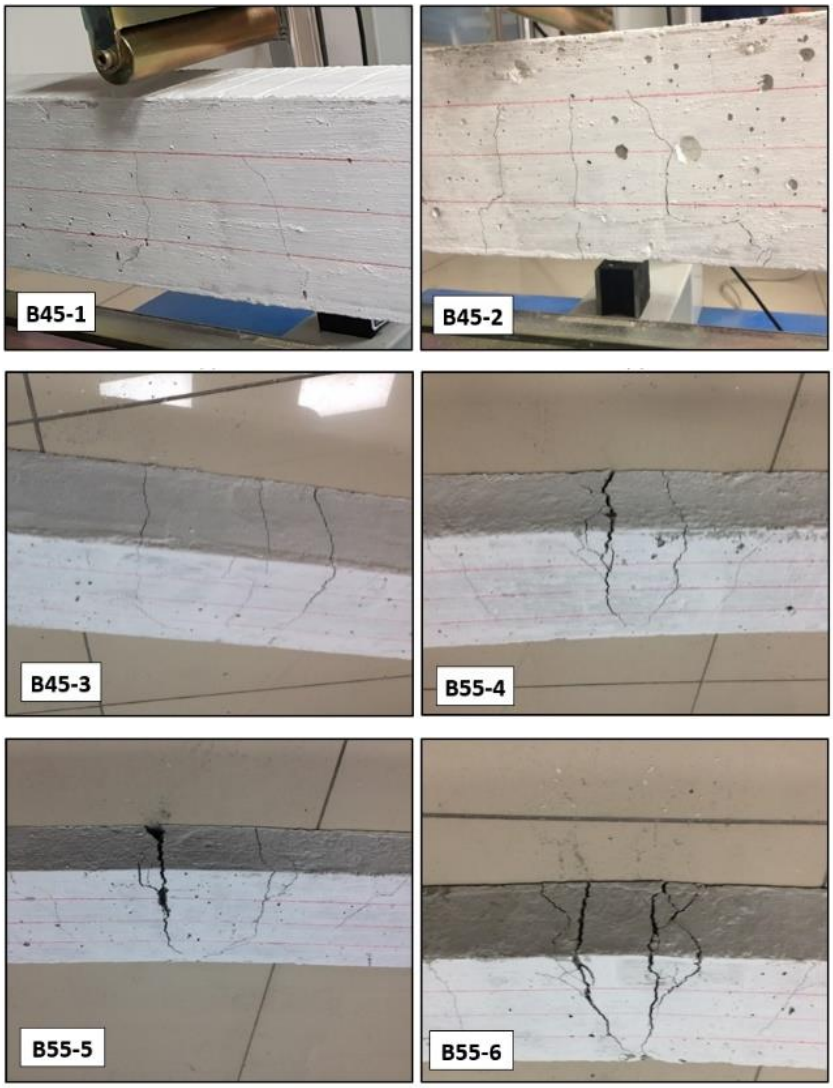

Fig. 3. Pre-created crack intensity of the specimens.

3. Experimental Results

Specimens RB55-0, B55-4, B55-5 and B55-6 collapsed in bending failure mode. Collapse of the specimens RB45-0, B45-1, B45-2 and B45-3 was predominant in bending failure mode, however large shear cracks also occurred in the beams. Fig. 5 is shown failure modes of specimens.

Obtained load-deflection curves of two group of specimens having concrete compressive strength of 45 MPa (RB45-0, B45-1, B45-2 and B45-3) and 55 MPa (RB55-0, B55-4, B55-5 and B55-6) were illustrated in Figs. 6 and 7, respectively.

Values of yielding load, ultimate load, yielding deflection and bending stiffness of the beam specimens were given in Table 2. Value of bending stiffness of the beams was obtained via dividing the yielding load by yielding deflection.

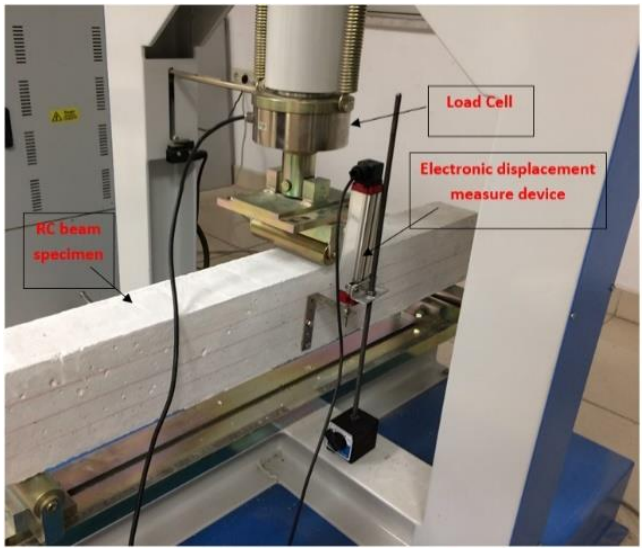

Fig. 4. Test setup.

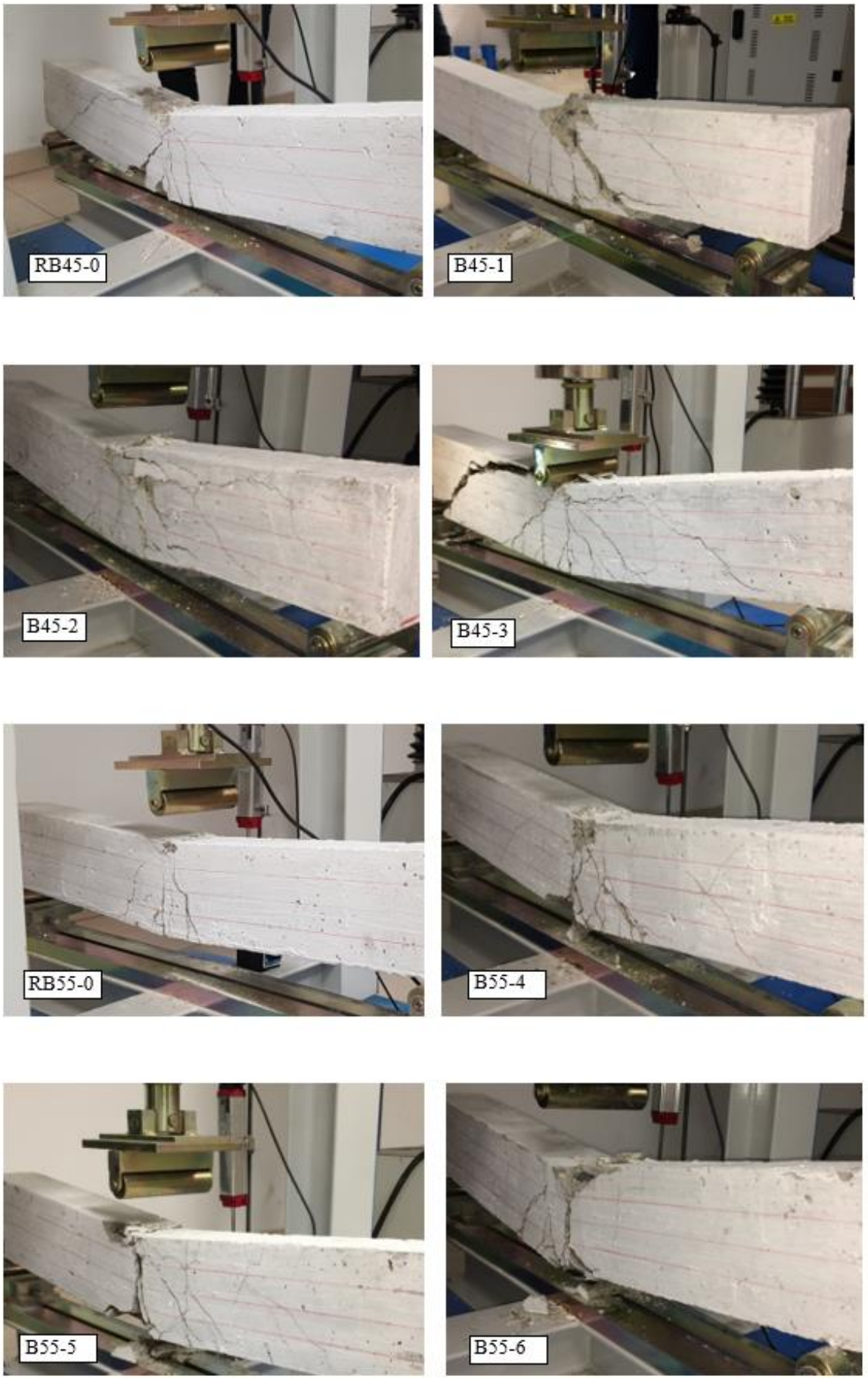

Fig. 5. Failure modes of specimens.

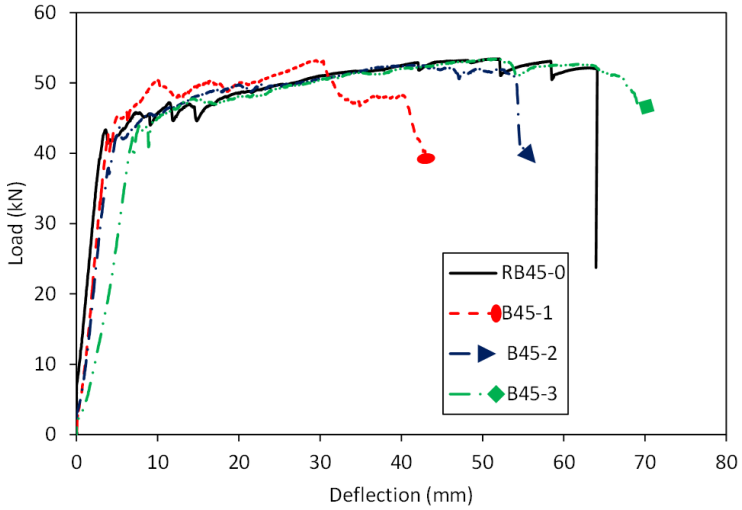

Fig. 6. Load-deflection curves of the specimens RB45-0, B45-1, B45-2 and B45-3.

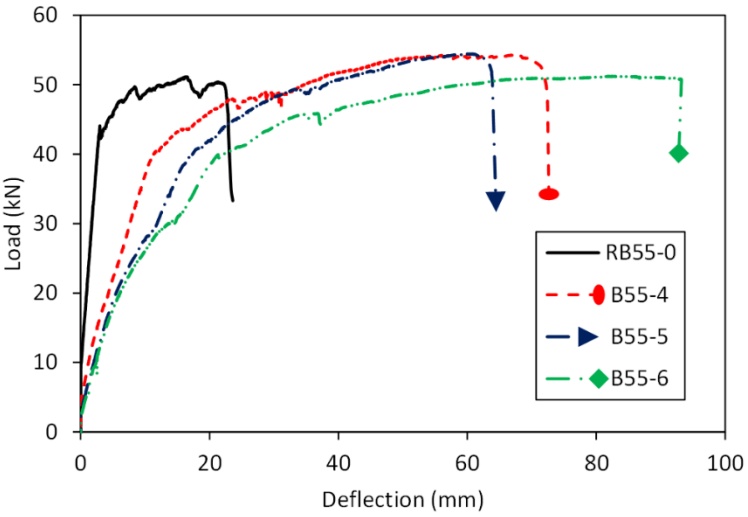

Fig. 7. Load-deflection curves of the specimens RB55-0, B55-4, B55-5 and B55-6.

Table 2. Experimental results of the specimens.

Specimen	Yielding load, *Py* (kN)	Ultimate load, *P*max (kN)	Yielding deflection, *δy* (mm)	Bending stiffness (kN/mm)
RB45-0	43.4	53.45	3.60	12.06
B45-1	42.8	53.20	3.89	11.00
B45-2	43.8	52.55	5.27	8.31
B45-3	42.2	53.43	6.91	6.11
RB55-0	44.1	51.17	2.97	14.85
B55-4	41.0	54.41	12.45	3.29
B55-5	40.9	54.47	18.28	2.24
B55-6	39.9	51.26	21.96	1.82

Table 3 shows the relative comparison of the beam specimens in terms of yielding load, ultimate load, yielding deflection and bending stiffness. Despite the pre-existing cracks in the beams B45-1, B45-2 and B45-3, the ultimate load and yield load values of these beams were almost the same as the values of the reference beam RB45-0. The difference compared to the reference beam was no more than 2% for ultimate load and 3% for yielding load. However, bending stiffness values decreased as the intensity of the pre-created cracks in beams increased. Difference of bending stiffness values with respect to reference beam was around 9%, 31% and 50% for the specimens B45-1, B45-2, and B45-3, respectively.

Table 3. Relative comparison of the experimental results of the specimens with respect to the reference beams.

Specimen	Reference beam	Ratio of the yielding load	Ratio of the ultimate load	Ratio of the yielding deflection	Ratio of the relative bending stiffness
B45-1	RB45-0	0.99	0.99	1.08	0.91
B45-2	RB45-0	1.01	0.98	1.46	0.69
B45-3	RB45-0	0.97	1.00	1.92	0.51
B55-4	RB55-0	0.93	1.06	4.19	0.22
B55-5	RB55-0	0.93	1.06	6.15	0.15
B55-6	RB55-0	0.90	1.00	7.39	0.12

During the study, since there was no considerable difference in terms of ultimate load and yielding load values when the specimens B45-1, B45-2, and B45-3 compared with the reference beam RB45-0, it was decided to increase the intensity of pre-created cracks on specimens B55-4, B55-5, and B55-6. Accordingly, 4th, 5th and 6th degrees of damage intensity were caused on the specimens B55-4, B55-5, and B55-6, respectively. Although there was larger pre-created damage in B55-4, B55-5, and B55-6 than B45-1, B45-2 and B45-3, the yielding load and ultimate load values obtained for the specimens B55-4, B55-5 and B55-6 weren't very different from those obtained for the reference beam RB55-0. There were mostly 9.5% and 6.4% difference in terms of yielding and ultimate load values, respectively.

Bending stiffness values of the specimens B55-4, B55-5 and B55-6 decreased as the pre-created cracks damage in beams increased. Difference of bending stiffness values with respect to reference beam RB55-0 was obtained around 78%, 85% and 88% for beams B55-4, B55-5, and B55-6, respectively. When the crack damages were created in those three beams, permanent vertical deflection occurred in the mid-span of the beams. Permanent vertical deflection of 9, 12 and 15 mm occurred in the beams B55-4, B55-5, and B55-6, respectively. It is thought that one of the reasons of the decrease in the bending stiffness is these permanent vertical deflections.

According to these results it is concluded that pre-created cracks with the studied intensity have an important effect especially in terms of bending stiffness of the beams. Therefore, in such cases, pre-created cracks damage should be considered when the deflection of RC beams is analyzed.

4. Conclusions

In this study, the effects of pre-created cracks, in compression zone of the section in the middle part of the span, on the behavior of RC beams were investigated experimentally. Compression strength of concrete and the intensity degree of pre-created cracks were adopted as test parameters. A total of 8 RC beams were tested under the effect of bending by three-point loading.

Conclusions obtained from the study summarized below.

- Specimens having a concrete compressive strength of 45 MPa, collapsed predominantly in bending failure mode, however, large shear cracks also occurred in the beams.
- Specimens having a concrete compressive strength of 55 MPa, collapsed in bending failure mode.
- Pre-cracked beams having a concrete compressive strength of 45 MPa, had closer values to the reference beam in terms of yielding load and ultimate load. The difference in terms of yielding load and ultimate load was at most 3% and 2%, respectively.
- Bending stiffness value of the pre-cracked beams having a concrete compressive strength of 45 MPa decreased as the intensity of pre-created cracks damage increased. Bending stiffness value of beams having intensity degree of 1, 2 and 3, was 9%, 31% and 50% less than the value of reference beam, respectively.
- Pre-cracked beams having a concrete compressive strength of 55 MPa, had closer values with the reference beam in terms of yielding load and ultimate load. The difference in terms of yielding load and ultimate load was at most 9.5% and 6.4%, respectively.
- Bending stiffness value of the pre-cracked beams having a concrete compressive strength of 55 MPa decreased as the intensity of pre-created cracks damage increased. Bending stiffness value of beams having intensity degree of 4, 5 and 6, was 78%, 85% and 88% less than the value of reference beam, respectively.
- Pre-created cracks with the studied intensity didn't have significant effect on RC beams in terms of yielding and ultimate load. However, there can be important decrease of the bending stiffness of the beams due to this kind of pre-created cracks damage.

Therefore, in such cases, it is concluded that pre-created cracks damage should be considered when the deflection of RC beams is analyzed.

For future studies, this kind of investigation can also be implemented for RC slabs. Specimens with a scale 1/3 to 1/5 are planned to be tested similarly in a future phase of this study using the same experimental method.

Acknowledgements

None declared.

Funding

The author received no financial support for the research, authorship, and/or publication of this manuscript.

Conflict of Interest

The author declared no potential conflicts of interest with respect to the research, authorship, and/or publication of this manuscript.

REFERENCES

Castel A, François R (2013). Calculation of the overall stiffness and irreversible deflection of cracked reinforced concrete beams. *Advances in Structural Engineering*, 16(12), 2035-2042.

Castel A, Vidal T, François R (2012). Finite-element modeling to calculate the overall stiffness of cracked reinforced concrete beams. *Journal of Structural Engineering*, 138(7), 889-898.

Castel A, Gilbert RI, Ranzi G (2013). Overall stiffness reduction of cracked reinforced concrete beams due to long term effects. *In Mechanics and Physics of Creep, Shrinkage, and Durability of Concrete*: *A Tribute to Zdeňk P. Bažant*, 443-450.

Castel A, Gilbert RI, Ranzi G (2014). Instantaneous stiffness of cracked reinforced concrete including steel-concrete interface damage and long-term effects. *Journal of Structural Engineering*, 140(6), 04014021.

Pan Z, Li B, Lu Z (2014). Effective shear stiffness of diagonally cracked reinforced concrete beams. *Engineering Structures*, 59, 95-103.

Rahman MA, Ayano T, Sakata K (1998). The use of physical phenomena to predict time effects in cracked reinforced concrete beams. *Magazine of Concrete Research*, 50(3), 219-227.

Sryh L, Forth J (2022). Long-term flexural behaviour of cracked reinforced concrete beams with recycled aggregate. *International Journal of Concrete Structures and Materials*, 16(1), 19.

Xu T, Castel A (2016). Modeling the dynamic stiffness of cracked reinforced concrete beams under low-amplitude vibration loads. *Journal of sound and Vibration*, 368, 135-147.

Xu T, Castel A, Gilbert RI (2018a). On the reliability of serviceability calculations for flexural cracked reinforced concrete beams. *Structures*, 13, 201-212.

Xu T, Huang J, Castel A, Zhao R, Yang C (2018b). Influence of steel–concrete bond damage on the dynamic stiffness of cracked reinforced concrete beams. *Advances in Structural Engineering*, 21(13), 1977-1989.

Xu T, Zhu L, Castel A, Gilbert RI (2018c). Assessing immediate and time-dependent instantaneous stiffness of cracked reinforced concrete beams using residual cracks. *Journal of Structural Engineering*, 144(4), 04018022.

Zhang S, Hamed E (2020,). Application of various creep analysis methods for estimating the time-dependent behavior of cracked concrete beams. *Structures,* 25, 127-137.